Structural phase transformation in K_2SeO_4

M. Iizumi,* J. D. Axe, and G. Shirane
Brookhaven National Laboratory,† Upton, New York 11973

K. Shimaoka
Ritsumeikan University, Kyoto, Japan
(Received 18 October 1976)

Successive phase transformations in K_2SeO_4 at $T_i = 130$ K and $T_c = 93$ K were studied by the neutron-scattering technique. The superlattice reflections in the intermediate phase were found to be incommensurate with the lattice periodicity. The wave vector characterizing the reflections is $\vec{q}_\delta = (1-\delta)\vec{a}^*/3$ with $\delta = 0.07$ at 122.5 K. The deviation δ decreases with decreasing temperature with an apparently discontinuous jump to zero at T_c. Below this temperature, the crystal remains commensurate and is known to be ferroelectric. The incommensurate-commensurate transition and the simultaneous occurrence of the commensurate phase and the spontaneous polarization are discussed using a Landau-type expansion of the free energy in which a term proportional to $Q^3(\vec{q}_\delta)P_z(\vec{q}_{3\delta})$ plays an essential role in driving the incommensurate-commensurate phase transformation and in inducing the spontaneous polarization. Here, $Q(\vec{q}_\delta)$ is the amplitude of the primary atomic displacements with wave vector $\vec{q}_\delta$ and $P_z(\vec{q}_{3\delta})$ is the polarization wave with wave vector $\vec{q}_{3\delta} = 3\delta(\vec{a}^*/3)$ and becomes the macroscopic polarization below T_c. Above T_i, a Σ_2 optic-phonon branch along $(\xi,0,0)$ shows a striking softening and $\omega_j(\vec{q})$ for $\vec{q} \sim (1/3,0,0)$ tends to zero at T_i. The softening results from a temperature-dependent decrease of the interlayer forces with ranges $a/2$ and a (a is one unit-cell length along the a axis) in the presence of strong and persisting forces with a range $3a/2$. The intensities of the soft phonon were measured about different reciprocal-lattice points and were used to determine the nature of the soft-phonon mode and suggest a coupled translation of potassium ions with rotational motion of SeO_4 groups to be the origin of the lattice instability.

I. INTRODUCTION

The concept of improper ferroelectrics[1,2] introduced independently by several authors in various forms has been applied successfully to understand the properties of many materials and the scope of this concept is still expanding. The variety of applications orignates from the differences in the primary order parameters and the different forms of the interaction terms through which the spontaneous polarization P is induced.

In the present paper we are going to report neutron-scattering studies of potassium selenate, K_2SeO_4, which reveals a new type of improper ferroelectric in which the primary order parameter is a lattice distortion Q_q with wave vector $\vec{q} = (\frac{1}{3},0,0)$ and the interaction term is

$$F_{\text{int}} = B(Q_q^3 + Q_{-q}^3)P_z . \quad (1)$$

Moreover, something beyond a simple extension and application of the existing theories on improper ferroelectrics is required in order to understand the phase transitions in this substance. We will see that the nature of the lattice instability in this compound leads to a phase which is incommensurate with the periodicity of the lattice and that the improper ferroelectric phase transformation occurs simultaneously with the "lock-in" transformation to a phase commensurate with the underlying lattice periodicity.

The incommensurate structural phase transformation is another current problem in the study of phase transitions. The significance of this type of phase transformation was emphasized recently in the layered transition-metal chalcogenides[3] in which the two-dimensional charge-density wave instability plays an essential role. More complicated successive phase changes between two commensurate phases through an intervening incommensurate phase were observed[4] in TTF-TCNQ (tetrathiafulvalene-tetracyanoquinodimethane) quite recently. The existence of incommensurate phases and transformations to commensurate phases have been already known in a few ferroelectrics such as $NaNO_2$,[5] and thiourea.[6] Therefore, the detailed neutron-scattering studies of the lattice instability in K_2SeO_4 will disclose an interesting type of the structural phase transition in which both the improper ferroelectric phase change and the incommensurate–commensurate phase change are combined together.

Potassium selenate was found by Aiki *et al.*[7,8] to undergo two successive phase transformations at $T_i = 129.5$ K and $T_c = 93$ K, the latter being a ferroelectric phase transformation with the spontaneous polarization along the c axis. The three phases separated by these two transformation temperatures will be designated as P (paraelectric), I (intermediate or incommensurate, as it will turn out), and F (ferroelectric) phases.

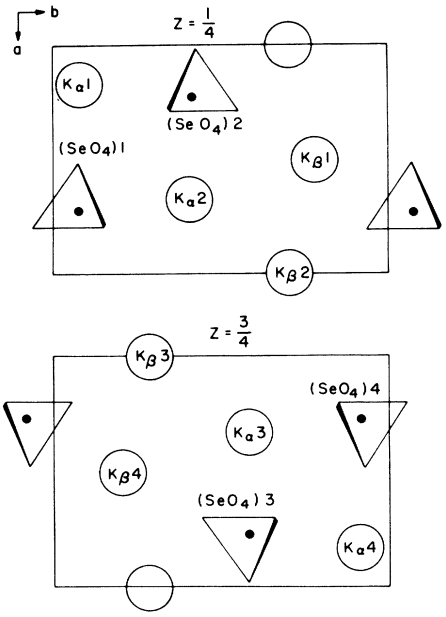

FIG. 1. Schematic structure of the P phase K_2SeO_4. Two levels along the c direction at heights $\frac{1}{4}$ and $\frac{3}{4}$ are shown separately. K_α and K_β are symmetrically nonequivalent potassium ions. Numbering identifies ions or groups.

The crystal structure of the P-phase[9] is isomorphous with β-K_2SO_4 with the orthorhombic space group $Pnam$ and is shown in Fig. 1. The structure is readily understood by considering that a unit cell consists of two levels along the c direction at heights $\frac{1}{4}$ and $\frac{3}{4}$ of $\vec{c}$. Each of the levels is shown separately in the figure. The unit cell contains four formula units, two sets of symmetrically nonequivalent potassium ions, K_α and K_β, and four SeO_4 groups, each of which we will treat as a single entity.

Below T_i, the x-ray diffraction[10,11] exhibited superlattice reflections which were characterized by the wave vector $\vec{q}_{1/3} = \frac{1}{3}\vec{a}^*$, where $\vec{a}^*$ is a vector reciprocal to $\vec{a}$, indicating that the superlattice structure has the unit-cell dimension three times longer along the $\vec{a}$ axis in the I phase than that in the P phase. The crystal structure of the I phase has been studied[11] by one of the present authors and others, who tentatively assigned $Pna2_1$ as the space group of the structure. Although this is a polar space group no spontaneous polarization was observed in the I phase, which leads one to conclude that the polarization is not reversible or that it is accidentally zero. The dielectric properties of the crystal above and below the second transformation temperature, T_c, were studied by Aiki *et al.*[8,12] They were found to be quite unusual in that the anomaly in the dielectric constant in the vicinity of T_c is small with a small Curie constant, 30 K. The spontaneous polarization below T_c is very small: 6.5×10^{-8} C/cm^2 at 80 K, though it exhibits a first-order jump. Thermal hysteresis was observed in the dielectric constant and spontaneous polarization. Although no structure determination has been attempted in the F-phase, it has been believed[11,13] that the crystal has an almost similar structure with the same orthorhombic space group $Pna2_1$ as the I phase, though Aiki *et al.*[6] suggested the monoclinic space group $P2_1$ in order to explain splitting observed in ESR spectra. Supposing the space group to be $Pna2_1$, we have the conceptual difficulty of explaining how the spontaneous polarization develops by passing through the phase transition where no symmetry element is lost. If the space group were $P2_1$, one would have to explain the development of the spontaneous polarization along the $\vec{c}$ axis by losing symmetry elements perpendicular to the $\vec{a}$ and $\vec{b}$ axes.

It is the purpose of the present neutron-scattering study to resolve this puzzling problem by measuring the structural and dynamical properties of the crystal in the three phases. We have found the right key to this problem lies in the incommensurately moderated structure in the I phase. We observed that the satellite reflections are not characterized by the wave vector $\vec{q}_{1/3}$ but by $\vec{q}_\delta = \frac{1}{3}(1-\delta)\vec{a}^*$ with δ changing with temperature between T_i and T_c and also that the deviation δ becomes zero at T_c and remains zero below T_c. This in principle removes the conceptual difficulty in the symmetry. There is a change in the symmetry at T_c. The remaining problem is to relate the occurrence of the spontaneous polarization to the incommensurate-commensurate phase transformation. For this purpose we have developed a Landau theory paying particular attention to the effect of higher-order coupling terms similar to those of Eq. (1). Observations of the symmetry nature of the soft mode above T_c substantiate this argument.

The dynamical fluctuations in the lattice in the vicinity of T_i have been investigated with x-ray scattering by Terauchi *et al.*[13] They observed temperature-dependent thermal diffuse scattering around $(\frac{2}{3},0,4)$ in reciprocal space and attributed it to the softening of a transverse optic phonon polarized along the $\vec{c}$ direction. The present neutron-scattering work confirms the existence of this soft phonon which belongs to the Σ_2 optic branch. The dispersion relation shows a striking softening around $\vec{q}_{1/3}$. Force-constant analysis suggests the origin of the lattice instability. An analysis of the intensities of the soft phonon measured at various points in the reciprocal lattice reveals the nature of the atomic displacements of the soft phonon.

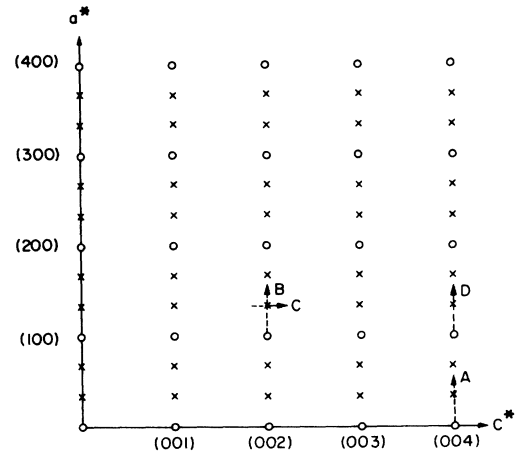

FIG. 2. [010] zone scattering plane in the reciprocal lattice of K_2SeO_4. Open circles indicate the reciprocal-lattice points in the P phase and ×'s locate the superlattice reflections found below T_i. Arrows indicate typical scans.

The format of this paper is as follows. All the experimental details are given in Sec. II. Observations of incommensurate satellite reflections and the transformation to the commensurate phase are presented in Sec. III. In Sec. IV we give the experimental results of lattice instability above T_i. This consists of three parts: the first part gives results on the temperature dependence of the dispersion relations of lattice vibrations; in Sec. IV B a force-constant analysis of the soft-phonon branch is given. Section IV C is concerned with the critical scattering in the vicinity of T_i. Theoretical matters are discussed in Secs. V and VII. In Sec. V the group-theoretical analysis of this type of structure is presented in order to help the analyses in the following two sections. In Sec. VII we develop a Landau theory of induced ferroelectricity. In Sec. VI we present the results of the dynamical structure analysis of the soft mode. Finally in Sec. VIII we will discuss the implication of the present results in a more general context.

II. EXPERIMENTAL

The single crystal, kindly provided by the Kyushu University group, was grown from the saturated aqueous solution by slow evaporation at 50 C. The volume of the crystal is about 4 cm^3. The crystal was mounted in an aluminum can filled with He gas and placed in a Cryogenics Associates CT-14 flow cryostat. The temperature was controlled within ±0.01 K. The mosaic spread of the crystal is very small ($\lesssim 10'$) and was not affected by the small cracks which developed on cycling through the phase transition several times.

The neutron-scattering experiments were performed on triple-axis spectrometers at the Brookhaven High Flux Beam Reactor. The majority of scans were made in the constant-Q mode with fixed incident neutron energies of 13.5 meV. A pyrolytic graphite filter was used to reduce the higher-order neutrons from the monochromator. Five meV neutrons with a Be filter were used for high-resolution studies. Horizontal collimation of 10 or 20 min was used depending on the resolution and intensity requirements. Collimation used is indicated in most of the following figures by four successive numbers connected with dashes. They indicate the in-pile, monochromator-to-sample, sample-to-analyzer, and analyzer-to-detector collimation, respectively.

All the scattering measurements were carried out in the [010] zone which is shown in Fig. 2. Open circles indicate the reciprocal-lattice points in the P phase and ×'s indicate the points where the satellite reflections appear below T_i.

Reflections and vectors in the reciprocal space are represented by reference to their respective unit cell, i.e., in the P phase $a^* = 2\pi/a$ and $c^* = 2\pi/c$ with $a = 7.588$ Å and $c = 5.973$ Å at 130 K; a^* is replaced by $a_L^* = \frac{1}{3}a^*$ in the I and F phases. Accordingly, the $(h\,0\,l)$ reflection in the P phase corresponds to the $(3h\,0\,l)$ reflection in the I and F phases.

III. INCOMMENSURATE SATELLITE REFLECTIONS

Satellite reflections of $(3h \pm 1\,0\,l)$ type were surveyed at 110 K and precise measurements revealed a slight deviation of peak positions in the reciprocal space from the commensurate points where the superlattice reflections were observed by x-ray measurements.[10,11,13] The incommensurate satellite reflections are characterized by a wave vector $\vec{q}_\delta = \frac{1}{3}(1-\delta)\vec{a}^*$ and $\delta = 0.045$ at 110 K. Figure 3 shows profiles of the elastic scattering scanned along the $\vec{a}^*$ axis (scan B in Fig. 2) at several temperatures between T_c and T_i. As is clear in this figure the deviation δ changes with temperature. Figure 4 summarizes the temperature dependence of δ. The deviation δ decreases with decreasing temperature and disappears discontinuously at T_c. Below this temperature the crystal remains commensurate. We can, therefore, conclude that the first phase transition at T_i is the transformation to an incommensurate structure and the second transition at T_c is an incommensurate-to-commensurate phase transformation.

Also clearly visible in Fig. 3 are weaker secondary peaks at wave vector $\vec{q}_{2\delta} = \frac{1}{3}(1+2\delta)\vec{a}^*$. Similar features were recently observed[3] in the incommen-

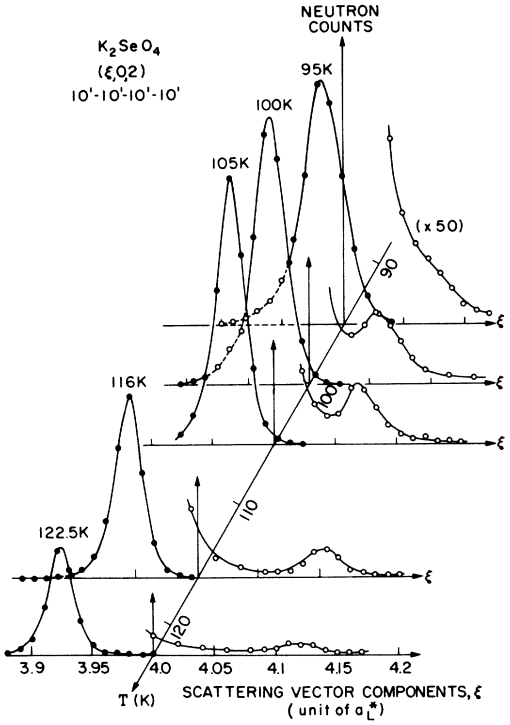

FIG. 3. Profiles of the elastic scattering scanned along [100] showing the incommensurate satellite reflection peaks at $\vec{q}_\delta = \frac{1}{3}(1-\delta)\vec{a}^*$ and secondary peaks at $\vec{q}_{2\delta} = \frac{1}{3}(1-2\delta)\vec{a}^*$. Open circles indicate multiplication by 50.

surate phase of $2H$-$TaSe_2$. As discussed in Ref. 3, these "2δ" peaks can be interpreted either as diffraction harmonic peaks arising from distortions with wave vector $\vec{q}_\delta$ or from secondary distortions with wave vector $\vec{q}_{2\delta}$. The δ vs T curve in Fig. 4 is probably slightly convex and thus of opposite curvature to that observed in $2H$-$TaSe_3$.[3]

Intensities of a satellite reflection ("δ" peak) and a representative fundamental reflection were measured as functions of temperature and the results are shown in Fig. 5. The intensity of the satellite reflection was measured allowing for the change of the peak positions with temperature. The intensity is proportional to $(T_i - T)^{0.8\pm0.1}$ down to 15 K below T_i. In Sec. VII it will be shown that the intensity of the satellite reflections are proportional to the square of the modulus of the order parameter for the I phase. The inset to Fig. 5 indicates detailed temperature dependence of the intensity at fixed points in Q space. (3.93, 0, 2) is a point where a satellite reflection appears just below T_i and (4, 0, 2) is a commensurate point. At (3.8, 0, 2) the intensity increases with decreasing temperature toward T_i and then intensity starts to decrease after T_i is passed. This behavior is typical of the critical scattering. From these measurements

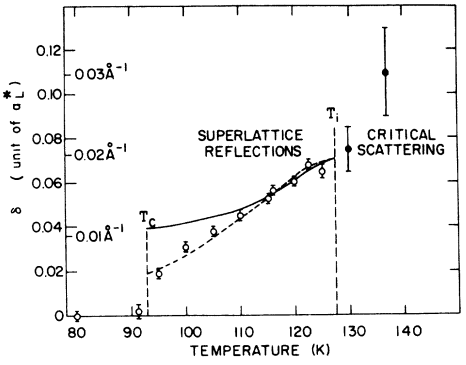

FIG. 4. Temperature dependence of δ. Those obtained from critical scattering peaks above T_i are also shown. Solid line is calculated by the Eq. (48) where the coefficient η_1^4 is set equal to 0.025 and the superlattice reflection intensity shown in Fig. 5 as a function of temperature is used as η_1^2. Dashed line is calculated by the Eq. (50) with $\gamma = 0.002$ and $T_i = 127.5$ K. For both cases δ_0 is taken to be 0.07.

the transition temperature T_i has been determined to be 127.5 ± 0.5 K. The satellite intensity evolves continuously at T_i indicating the transition is of second order. The intensity of the fundamental Bragg reflection does not change on passing through T_i. Also every effort to see discontinuous jump in Bragg intensities at T_c has failed. Instead a broad hysteresis-like behavior was observed as shown in Fig. 5. Aiki *et al.*[7,12] have observed hysteresis in the spontaneous polarization and dielectric constant which changes with the rate of temperature change and with the specimen. The change in intensity of the fundamental reflection above and below T_c, also shown in Fig. 5, may be explained by the extinction effect due to the development of domains.

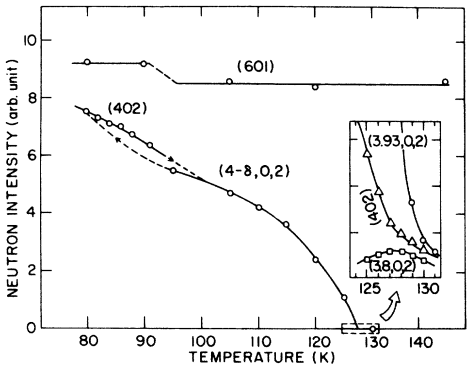

FIG. 5. Intensities of a fundamental reflection (601) and a satellite reflection (4 −δ 0 2) vs temperature. Inset shows details of temperature change of intensities at a few fixed points around a satellite point (4−δ, 0, 2).

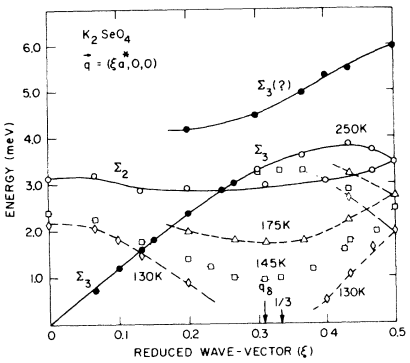

FIG. 6. Dispersion relations of transverse modes propagating in the [100] direction. Parts of the dispersion relations indicated by solid circles are almost temperature independent.

IV. LATTICE INSTABILITY ABOVE T_i

The lattice instability manifests itself in temperature-dependent scattering of neutrons above T_i. The nature of the scattering was studied in two temperature ranges. At temperatures not close to T_i we found a phonon mode with a temperature-dependent frequency at about $\vec{q}=(\frac{1}{3},0,0)$ and its dispersion relation was studied. Then at temperatures just above T_i the critical scattering around $(\frac{1}{3},0,0)$ was studied as a function of q, ω, and T.

A. Phonon dispersion relations

Some preliminary measurements disclosed the existence of a strongly temperature-dependent excitation with the wave vector $\vec{q}\cong(\frac{1}{3},0,0)$. The strongest scattering within the reach of 13.5 meV incident neutrons was observed at $(\frac{4}{3},0,4)$ where the satellite reflection below T_i was also the strongest of the reflections within the reach. The excitation energy was traced as a function of $\vec{q}$ and the whole branch from the zone center to the zone boundary was observed at several temperatures. The results are shown in Fig. 6. The branch is labeled of Σ_2 symmetry as is established later in Sec. V. The dispersion relation of the transverse Σ_3 acoustic phonon and a part of a transverse optic phonon branch (perhaps of Σ_3 symmetry) are also shown in the figure. They showed strong intensity about (0,0,4). Parts of the dispersion relations indicated by solid circles are almost temperature independent. The Σ_2 branch is degenerate with the Σ_3 acoustic branch at the zone boundary, and shows a dispersion relation which is almost flat and softens as a whole at high temperatures. As the transition temperature T_i is approached the softening becomes conspicuous particularly around $\vec{q}_{1/3}$ but extends over wide range in q and even to the part of the TA branch near zone boundary. The squares of the phonon energies $\hbar\omega(\vec{q})$ as measured by the position of the peak in the one-phonon scattering at the zone center, $\vec{q}_\Gamma=(0,0,0)$, at $\vec{q}_\delta=(0.31,0,0)$ and at the zone boundary, $\vec{q}_X=(0.5,0,0)$, are plotted in Fig. 7 as a function of temperature. Near T_i the one phonon scattering of the soft phonon may peak at an energy considerably shifted from the real part of the phonon self-energy $\hbar\omega_0(\vec{q}_\delta)$ due to damping effects. The $[\hbar\omega_0(\vec{q}_\delta)]^2$ vs T curve is thus likely to be more nearly linear than indicated by the figure. The dispersion relation in the direction perpendicular to Σ is measured by fixing the x component of the wave vector to $0.31a^*$. The results shown in Fig. 8 indicate that the softening is confined to a more restricted region in $\vec{q}$ space in this direction. The fitting of the dispersion surface measured at 130 K to the expression

$$[\hbar\omega(\vec{q})]^2=[\hbar\omega(\vec{q}_0)]^2+\beta_1'(q_x-q_0)^2+\beta_2'q_y^2+\beta_3'q_z^2, \qquad (2)$$

gives

$$\beta_1'=110\ \text{meV}^2\text{A}^2,$$

$$\beta_2'=570\ \text{meV}^2\text{A}^2,\quad \hbar\omega(\vec{q}_0)=0.17\ \text{meV}, \qquad (3)$$

where $\vec{q}_0$ is taken to be (0.3, 0, 0). This anisotropy implies that the softening of the frequency is restricted to a kind of motion in which planes or layers perpendicular to $\vec{a}$ take part as a whole. Lattice vibrations in which phases of atomic motion are not uniform on the planes cost higher energy.

B. Interlayer force constant analysis

The degeneracy of the Σ_2 optic branch with the Σ_3 acoustic phonon and the coincidence of the absolute value of the slope at the zone boundary establish that the Σ_2 branch is an extension of the Σ_3

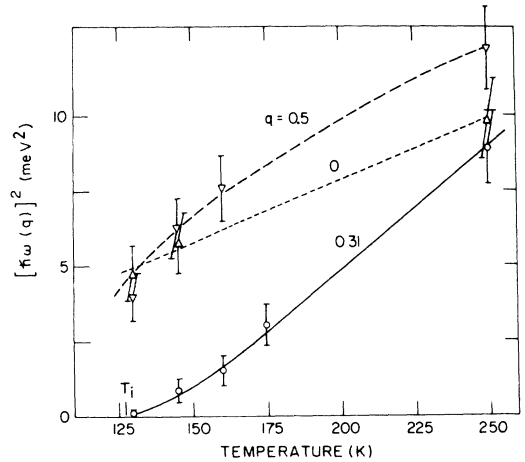

FIG. 7. Squares of the phonon energies at the zone center, $\vec{q}_\Gamma=(0,0,0)$ at $\vec{q}_\delta=(0.31,0,0)$ and at the zone boundary, $\vec{q}_X=(0.5,0,0)$ as a function of temperature.

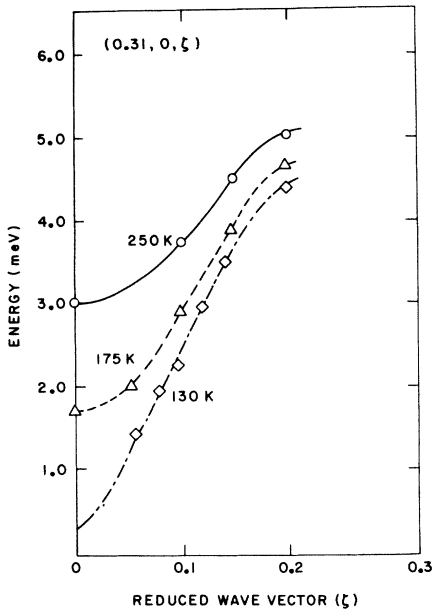

FIG. 8. Dispersion relation of the soft mode along the line passing through (0.31, 0, 0) in the [001] direction.

acoustic branch in an extended zone which is doubled along the $\vec{a}^*$ axis. Figure 9 shows the Σ_3 and Σ_2 branches in the extended zone scheme. This extended zone corresponds to the periodicity of $\frac{1}{2}a$ along $\vec{a}$ in the lattice space. The glide plane $\{\sigma_y|\frac{1}{2}\vec{a}+\frac{1}{2}\vec{b}\}$ assures this pseudoperiodicity for the lattice vibration propagating along $\vec{a}$, where σ_y is the reflection in the plane normal to the y axis and

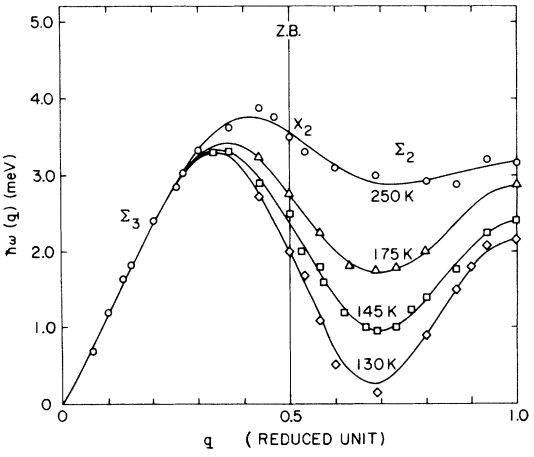

FIG. 9. Dispersion relation of the Σ_2 soft mode along with the Σ_3 acoustic mode plotted in an extended zone which is doubled along the $\vec{a}^*$ axis. Z.B. indicates the original zone boundary. Solid lines show the results of fitting of Eq. (4) to the data. Fictitious effective force constants, F_n, coupling layers in the crystal separated by a distance equal to $\frac{1}{2}na$ are derived from the fitting.

TABLE I. Interlayer force constants. These were determined by the least-square fitting of Eq. (4) to the dispersion curves in the extended zone shown in Fig. 9. Errors in the values are about 0.20 meV^2.

	F_n (meV^2)			
n	130 K	145 K	175 K	250 K
1	−1.75	−1.14	0.19	2.41
2	1.41	1.83	2.14	4.00
3	4.45	4.27	4.18	3.00
4	0.58	0.28	−0.01	−0.25
5	−0.30	−0.27	−0.27	−0.45
6	−0.60	−0.44	−0.38	−0.14

$\frac{1}{2}\vec{a}+\frac{1}{2}\vec{b}$ is a fractional translation. (This is similar to the case of phonons propagating along the $\vec{c}$ axis of the hexagonal close-packed lattice.) Then since the dispersion relation is periodic in this extended zone, we can characterize the dispersion relation by the Fourier series,

$$[\hbar\omega(\xi)]^2 = \sum_n F_n(1-\cos n\pi\xi), \tag{4}$$

in which ξ is the x component of the wave vector in the reduced unit and the coefficients F_n correspond to fictitious effective force constants coupling layers in the crystal separated by a distance equal to $\frac{1}{2}na$. Expression (4) with six terms was least-square-fitted to the dispersion relations at each temperature. Sets of the force constants obtained are given in Table I and are shown in Fig. 10 as

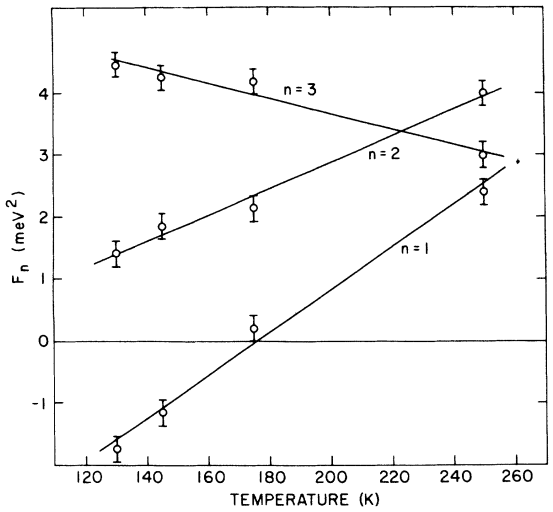

FIG. 10. Temperature dependence of the nearest-, second-, and third-neighbor interlayer force constants. Force constants beyond $n=3$ are insignificant. Decrease of both F_1 and F_2 in the presence of a strong and persisting force F_3 results in the softening of phonon energy at about $(\frac{1}{3}, 0, 0)$.

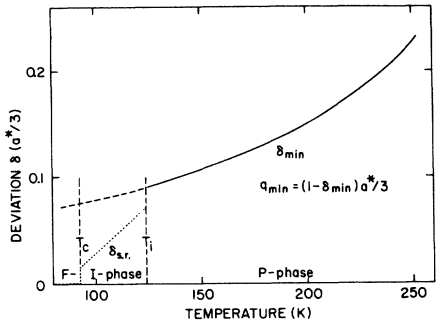

FIG. 11. Temperature change of the minimum position of the fitted dispersion curve. Deviation of the minimum position from $\vec{q}_{1/3}=\frac{1}{3}\vec{a}^*$ is plotted in units of $\frac{1}{3}a^*$ as a function of temperature. This "dynamical" δ is extrapolated to the I phase and is compared with the "static" δ obtained from the peak position of the superlattice reflections (Fig. 4). Discrepancy suggests some factor pushing the "static" δ towards zero (a commensurate phase).

functions of T. The force constants beyond $n=3$ are insignificant and are not shown in the figure. The fitted dispersion curves are shown in Fig. 9. The softening of the dispersion relation is well described by the linear temperature-dependence of the force constants. The force constant between nearest-neighbor layers, F_1, decreases linearly with decreasing temperature and changes its sign at about 175 K. F_2 is larger than F_1 and also decreases as the temperature is lowered. In contrast the force constant between the third-neighbor layer, F_3, is strong and increases only slightly with decreasing temperature. At temperatures just above T_i, F_3 becomes the predominant component. Note that F_3 alone produces a phonon instability at $\xi=\frac{2}{3}$. Thus the softening of the Σ_2 phonon in this crystal results from the temperature-dependent decrease of both F_1 and F_2 in the presence of a strong and persisting force with a range $\frac{3}{2}a$ with magnitude F_3.

The minimum of the dispersion curve defines the wave vector $\vec{q}_{\min}$ for which the lattice vibration is most unstable. This was calculated from $d\omega^2(\vec{q})/dq=0$ in which $\omega^2(\vec{q})$ is given by the expression (4) with the first three dominant terms with the linear temperature-dependence of the force constants substituted in the expression. The result is shown in Fig. 11, where the deviation of the minimum point from $\vec{q}_{1/3}$, $\delta_{\min}$ is plotted in units of $\frac{1}{3}a^*$. In the figure comparison is made between $\delta_{\min}$ extrapolated into I phase and $\delta_{s.r.}$ obtained from the satellite reflections and shown in Fig. 4. At the second-order transition temperature T_i both deviations presumably coincide. This disagreement is attributable to errors in estimating $\delta_{\min}$. Below T_i $\delta_{s.r.}$ appreciably departs from the intrinsic tendency given by $\delta_{\min}$. In Sec. VII we will see that higher-order terms in a free-energy expansion ("umklapp" terms) are responsible for this increasing tendency toward commensurability.

C. Critical scattering

X-ray scattering[13] has revealed critical scattering around $\vec{q}_{1/3}$ just above T_i. The strength of the neutron-scattering method is to disclose the energy dependence of this scattering. The energy profiles of the scattering were measured at $(\frac{4}{3},0,2)$ at three temperatures above T_i and are shown in Fig. 12 after subtracting the incoherent elastic scattering. At high temperature ($T\gtrsim 145$ K) the scattering consists of well-defined phonon sidebands. As the transformation temperature is approached from above, the phonon sidebands disappear and the critical scattering peaks at $E=0$. In between there is weak evidence for a three-peak structure at 137 K. The unusual width in the wings of the energy profile at 130 K also suggests the presence of more than one relaxation time. A high resolution scan of the central part of the scattering shown in the inset to Fig. 12 revealed no detectable energy width. For convenience's sake the spectra will be considered in the following to consist of the sharp central peak region and the residual phononlike

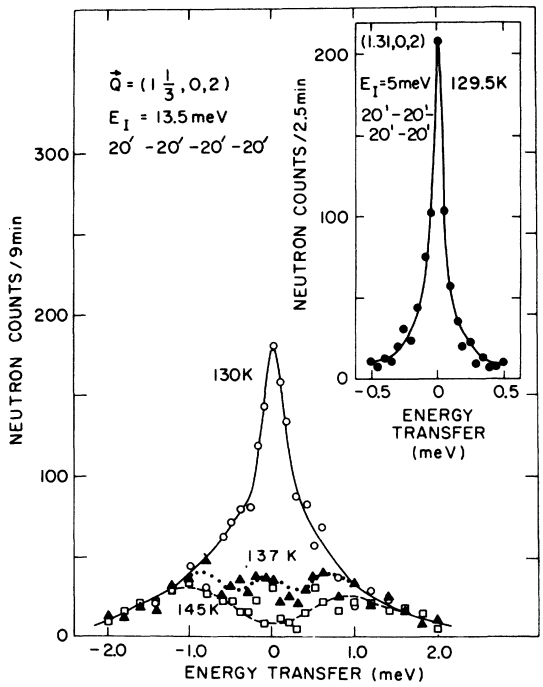

FIG. 12. Energy profiles of the critical scattering at $(\frac{4}{3},0,2)$. Incoherent scattering has been subtracted. Inset shows the high resolution measurement of the central part of the scattering at (1.31, 0, 2).

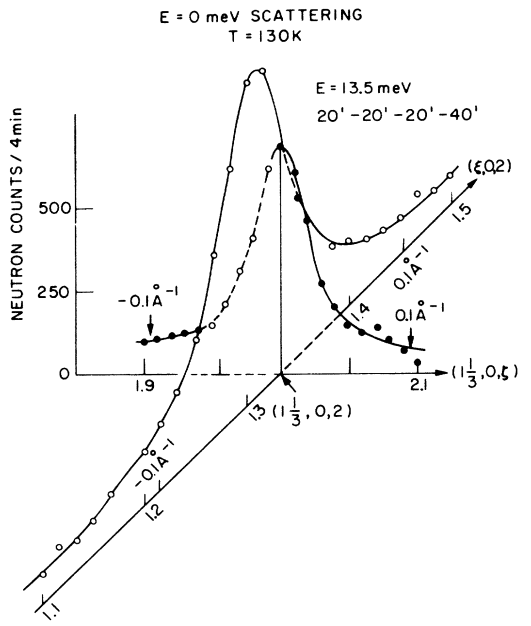

FIG. 13. $E=0$ scattering distribution around $(\frac{4}{3},0,2)$ at 130 K. Scattering peaks at an incommensurate position along $\vec{a}^*$ axis. FWHM's are 0.064 $Å^{-1}$ along $\vec{a}^*$ and 0.048 $Å^{-1}$ along $\vec{c}^*$.

part. But any further attempts have not been made to characterize the central peak.

Figure 13 shows the $E=0$ scattering distribution around $(\frac{4}{3},0,2)$ at 130 K (scans B and C in Fig. 2). The scattering peaks at an incommensurate position along $\vec{a}^*$ but precisely along the $\vec{c}^*$ axis. The distribution is somewhat anisotropic, the FWHM (full width at half maximum) being 0.064 $Å^{-1}$ along $\vec{a}^*$ and 0.048 $Å^{-1}$ along $\vec{c}^*$ at 130 K. This $E=0$ neutron-scattering distribution differs markedly from the x-ray diffuse scattering,[13] which consists of diffuse streaks extending from $\vec{q}=0$ to the zone boundary along $\vec{a}^*$, but very narrow (FWHM of 0.006 $Å^{-1}$ at $T=T_i+2$K).[14] The disagreement results from the different energy sensitivity of the methods. The $E=0$ neutron scattering sees intensity which falls within a finite energy resolution around $E=0$, while the x-ray method observes an integrated intensity of whole spectrum. Near T_i the $E=0$ neutron scattering gives a distribution of the central peak which is confined in a fairly narrow region around $\vec{q}_6$. On the other hand, the critical scattering observed by x rays reflects the anisotropy of the soft phonon dispersion as given in (3).

Figure 14 shows the $E=0$ scattering measured at several temperatures along two perpendicular directions (B and C in Fig. 2) with higher resolution. Peak positions of $(\xi,0,2)$ distribution tend to shift to smaller q_6 as temperature decreases. The values of δ of this critical scattering have already been shown in Fig. 4. Although they have larger errors compared with those for the superlattice reflections, they seem to change continuously through T_i. The $E=0$ intensity at a fixed point in the reciprocal lattice does not follow linear I^{-1} vs T nor linear $I^{-1/2}$ vs T relations. According to the phenomenological formula[15] which has been used with some success to explain the three peak structure in $SrTiO_3$ and other materials, the intensities of the central peak approximately change as $(T-T_i)^{-2}$ and the total intensity as $(T-T_i)^{-1}$. The $E=0$ neutron scattering which consists of the total central peak intensity and small fraction of phonon components does not satisfy this first sum rule adequately. The diffuse scattering intensity obtained by the x-ray method,[13] however, changes like $(T-T_i)^{-1}$ because the total phonon plus central peak intensity is observed in this case.

V. SYMMETRY ANALYSIS OF THE NORMAL MODES

The purposes of this section are: (a) to establish the relationship between changes in the crystal space group symmetry at the phase transformation and the soft mode driving the phase changes and; (b) to derive the symmetry-adopted eigenvectors of the soft mode which are required in order to carry out the dynamical structure analysis in Sec. VI. The unit cell of potassium selenate above T_i contains four formula units, each of which consists of seven atoms. There are, therefore, 84 normal modes for each $\vec{q}$. It is, however, reasonable to neglect the internal-vibrational degrees of freedom in the SeO_4 groups for our present purposes. Then we have 48 degrees of freedom, 18 of which are rotational motions of SeO_4 groups.

Symmetry elements of the space group $Pnam$-D_{2h}^{16} are given in Table II. We restrict our analysis to $\vec{q}_\Gamma=(0,0,0)$, $\vec{q}_\Sigma=(q_1,0,0)$, and $\vec{q}_X=(0.5,0,0)$. The

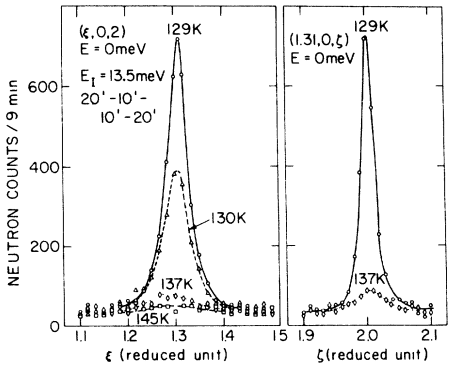

FIG. 14. $E=0$ scattering scans along the $\vec{a}^*$ and $\vec{c}^*$ axes at several temperatures.

TABLE II. Symmetry operation of the space group D_{2h}^{16}-*Pnam*. Transformations have been made on the original definitions given by Kovalev (Ref. 16) and the International Tables (Ref. 17) which adopt different setting of axes.

Kovalev (Ref. 16)	Seitz	International Tables (Ref. 17)
h_1	$\{E\|0\}$	x, y, z
h_2	$\{C_{2x}\|\frac{1}{2}\vec{a}+\frac{1}{2}\vec{b}+\frac{1}{2}\vec{c}\}$	$\frac{1}{2}+x, \frac{1}{2}-y, \frac{1}{2}-z$
h_3	$\{C_{2y}\|\frac{1}{2}\vec{a}+\frac{1}{2}\vec{b}\}$	$\frac{1}{2}-x, \frac{1}{2}+y, \bar{z}$
h_4	$\{C_{2z}\|\frac{1}{2}\vec{c}\}$	$\bar{x}, \bar{y}, \frac{1}{2}+z$
h_{25}	$\{I\|0\}$	$\bar{x}, \bar{y}, \bar{z}$
h_{26}	$\{\sigma_x\|\frac{1}{2}\vec{a}+\frac{1}{2}\vec{b}+\frac{1}{2}\vec{c}\}$	$\frac{1}{2}-x, \frac{1}{2}+y, \frac{1}{2}+z$
h_{27}	$\{\sigma_y\|\frac{1}{2}\vec{a}+\frac{1}{2}\vec{b}\}$	$\frac{1}{2}+x, \frac{1}{2}-y, z$
h_{28}	$\{\sigma_z\|\frac{1}{2}\vec{c}\}$	$x, y, \frac{1}{2}-z$

irreducible representations of the point group of q_Σ are given in Table III, which is taken from the table compiled by Kovalev[16] with a change of notation of the representations for convenience.

The decomposition of representations in 48-dimensional displacement space gives the following results: (i) at Γ point

$$7\Gamma_1+5\Gamma_2+5\Gamma_3+7\Gamma_4+5\Gamma_5+7\Gamma_6+7\Gamma_7+5\Gamma_8;$$

(ii) on Σ line

$$14\Sigma_1+10\Sigma_2+10\Sigma_3+14\Sigma_4; \tag{5}$$

(iii) at X point

$$14X_1+10X_2,$$

where Γ_i and X_i correspond to $\hat{\tau}^i$ at $\vec{k}_{19}$ and $\vec{k}_{21}$ for D_{2h}^{16} in Kovalev's table. X_1 and X_2 are doubly degenerate modes. The compatibility relations are shown in Table IV.

The transverse acoustic mode with the polarization vectors in the z direction transforms according to the Σ_3 irreducible representation. Application of the compatibility relations to the measured dispersion relation given in Fig. 10 leads to the conclusion that the soft mode transforms according to Σ_2. The optic branch which is polar along z at Γ belongs to Σ_3.

TABLE III. Irreducible representation of the group at Σ: $(q, 0, 0)$.

	$\{E\|0\}$	$\{C_{2x}\|\frac{1}{2}\vec{a}+\frac{1}{2}\vec{b}+\frac{1}{2}\vec{c}\}$	$\{\sigma_y\|\frac{1}{2}\vec{a}+\frac{1}{2}\vec{b}\}$	$\{\sigma_z\|\frac{1}{2}\vec{c}\}$
Σ_1	1	1	1	1
Σ_2	1	1	−1	−1
Σ_3	1	−1	1	−1
Σ_4	1	−1	−1	1

The symmetry-adopted eigenvectors which transform according to Σ_2 are

$$\begin{aligned}
&\vec{s}_1=(\vec{T}_a,0,0,0), \quad \vec{s}_2=(\vec{T}_s,0,0,0), \quad \vec{s}_3=(0,\vec{T}_a,0,0),\\
&\vec{s}_4=(0,\vec{T}_s,0,0), \quad \vec{s}_5=(0,0,\vec{T}_a,0), \quad \vec{s}_6=(0,0,\vec{T}_s,0),\\
&\vec{s}_7=(0,0,0,\vec{R}_a^x), \quad \vec{s}_8=(0,0,0,\vec{R}_s^x), \quad \vec{s}_9=(0,0,0,\vec{R}_a^y),\\
&\vec{s}_{10}=(0,0,0,\vec{R}_s^y),
\end{aligned} \tag{6}$$

where each of the four components is a column vector of 12 components representing the translational motions of K_α ions, K_β ions, and SeO_4 groups and the rotational motions of the SeO_4 groups, respectively. Translational component vectors $\vec{T}_a$ and $\vec{T}_s$ are defined as

$$\begin{aligned}
\vec{T}_a&=\tfrac{1}{2}(001,00-1,00-1,001),\\
\vec{T}_s&=\tfrac{1}{2}(001,00-1,001,00-1),
\end{aligned} \tag{7}$$

where the four 3-vectors describe the displacements of the four atoms or groups, for example $(K_\alpha 1, K_\alpha 2, K_\alpha 3, K_\alpha 4)$. Three components in each division indicate x, y, and z components of the displacement of atoms or groups. The rotational motions of SeO_4 groups are described by angles of rotation of each group around x, y, and z axes. They can be written in the same form as the translational vectors:

$$\begin{aligned}
\vec{R}_a^x&=\tfrac{1}{2}(100,100,-100,-100),\\
\vec{R}_s^x&=\tfrac{1}{2}(100,100,100,100),\\
\vec{R}_a^y&=\tfrac{1}{2}(010,0-10,010,0-10),\\
\vec{R}_s^y&=\tfrac{1}{2}(010,0-10,0-10,010).
\end{aligned} \tag{8}$$

In Eqs. (7) and (8) the suffixes s and a indicate that the displacements are symmetric or antisymme-

TABLE IV. Compatibility relations at Γ $(0, 0, 0)$ and at X $(\frac{1}{2}, 0, 0)$. Irreducible representations Γ_1 to Γ_8 correspond to $\hat{\tau}_1$ to $\hat{\tau}_8$ for $T32$ and X_1, X_2 correspond to $\hat{\tau}_1$, $\hat{\tau}_2$ for $T70$ in Kovalev's compilation (Ref. 16), A_g, etc. are the Mulliken notation of the representation.

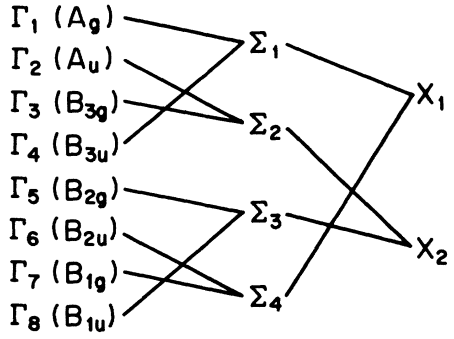

tric for the inversion, for instance,

$$T_{sz}(\bar{k}) = -T_{sz}(k) \quad \text{and} \quad T_{az}(\bar{k}) = T_{az}(k), \tag{9}$$

where $\bar{k}$ is the label of the atom to which the atom k is transformed by the inversion. The symmetry-adopted modes $\vec{s}_1$ and $\vec{s}_2$ are illustrated in Fig. 15 together with one of the rotational modes $\vec{s}_{10}$.

The eigenvectors of the Σ_2 mode are linear combinations of these symmetry-adopted eigenvectors

$$\vec{e}(\vec{q}, \Sigma_2, j) = \sum_{\lambda=1}^{10} S_{j\lambda}(\vec{q})\, \vec{s}_\lambda, \quad j = 1, 2, \ldots, 10, \tag{10}$$

where j is the branch index. The symmetry coordinate component $S_{j\lambda}(\vec{q})$ represents the fraction of the $\vec{s}_\lambda$ mode in the jth normal mode at $\vec{q}$. Note that time-reversal symmetry requires that

$$\vec{e}^*(k\,|\,\vec{q}, \Sigma_2, j) = \vec{e}(\bar{k}\,|\,\vec{q}, \Sigma_2, j). \tag{11}$$

With our choice of the symmetry-adopted eigenvectors (6), the relation (11) is satisfied by

$$\begin{aligned} &S_{j\lambda}(\vec{q}) = S^*_{j\lambda}(\vec{q}) \text{ for } \lambda = 1, 3, \ldots, 9, \\ &S_{j\lambda}(\vec{q}) = -S^*_{j\lambda}(\vec{q}) \text{ for } \lambda = 2, 4, \ldots, 10. \end{aligned} \tag{12}$$

The displacement of the pth atom in the kth group in the lth unit cell is given by

$$\begin{aligned} u(lkp\,|\,\vec{q}\,\Sigma_2 j) = M_p^{-1/2} \sum_{\vec{q}} Q(\vec{q}\,\Sigma_2 j) \\ \times [\vec{e}(k\,|\,\vec{q}\,\Sigma_2 j) \\ + \vec{e}(k'\,|\,\vec{q}\,\Sigma_2 j) \times \vec{X}(kp)]\, e^{i\vec{q}\cdot\vec{X}(lk)}, \end{aligned} \tag{13}$$

where k' indicates the rotational component of group k, $\vec{X}(lk)$ is the position of center of mass of the kth group in the lattice, $\vec{X}(kp)$ is the position of pth atom with respect to the center of mass of the kth group, M_p is the mass of pth atom and $Q(\vec{q}\,\Sigma_2 j)$ is the amplitude of the mode.

In order to investigate what space group the crystal assumes when a Σ_2 mode condenses with the wave vector $\vec{q}_{1/3}$, it is enough to consider a minimum subset of atoms with the group properties. For example, consider ($K_\alpha 1, K_\alpha 2, K_\alpha 3, K_\alpha 4$). Displacements of these atoms are

$$\vec{u}(lk) = Q_{\vec{q}}\, \vec{e}(k\,|\,\vec{q})\, e^{i\vec{q}\cdot\vec{X}(lk)} + \text{c.c.}, \tag{14}$$

with

$$\vec{e}(\vec{q}) = \alpha(\vec{q})\vec{T}_a + i\beta(\vec{q})\vec{T}_s, \tag{15}$$

where $\vec{T}_a$ and $\vec{T}_s$ are defined in Eq. (7) and are illustrated in Fig. 15. $\alpha(q)$ and $\beta(q)$ are real by the properties given in Eq. (12). c.c. in Eq. (14) indicates the complex conjugate of the first term. The amplitude factor is in general complex

$$Q_{\vec{q}} = \tfrac{1}{2}\eta e^{i\phi} \tag{16}$$

and the displacements are given by

$$\begin{aligned} u_z(lk) = \eta\{&\alpha T_{az}(k) \cos[\vec{q}\cdot\vec{x}(lk) + \phi] \\ &- \beta T_{sz}(k) \sin[\vec{q}\cdot\vec{x}(lk) + \phi]\}. \end{aligned} \tag{17}$$

The cos and sin terms have the same transformation properties, so we will only consider the symmetry properties of the cos term in detail. In Fig. 16 we show the displacements of K_α atoms in the unit cell of the F phase for the special choice of $\phi = 0$ and $\frac{1}{2}\pi$. $\phi = \frac{1}{3}\pi$ and $\frac{1}{6}\pi$ also gives the same results. For these special choices of the phase the atomic displacements take either of three values,

$$\begin{aligned} &a = \cos\tfrac{2}{3}\pi x_1, \quad b = \cos\tfrac{2}{3}\pi(\tfrac{1}{2} - x_1), \\ &c = \cos\tfrac{2}{3}\pi(\tfrac{1}{2} + x_1) \end{aligned} \tag{18}$$

for $\phi = 0$ and

$$\begin{aligned} &a' = \sin\tfrac{2}{3}\pi x_1, \quad b' = \sin\tfrac{2}{3}\pi(\tfrac{1}{2} - x_1), \\ &c' = \sin\tfrac{2}{3}\pi(\tfrac{1}{2} - x_1) \end{aligned} \tag{19}$$

for $\phi = \frac{1}{2}\pi$. Here x_1 is the x coordinate of $K_\alpha 1$ atom. The space groups of the distorted structures are

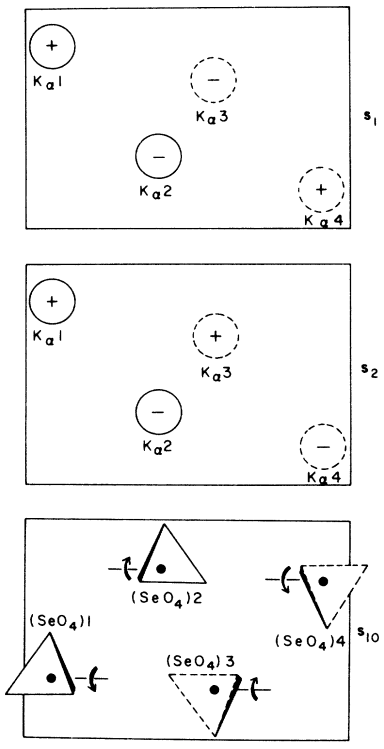

FIG. 15. Σ_2-type symmetry-adopted eigenvectors. There are ten of them. Only $\vec{s}_1$, $\vec{s}_2$, and $\vec{s}_{10}$ are shown here. Plus and minus signs indicate displacements in the c direction. Arrows in the bottom figure indicate rotation of SeO_4 groups around axes parallel to the b axis.

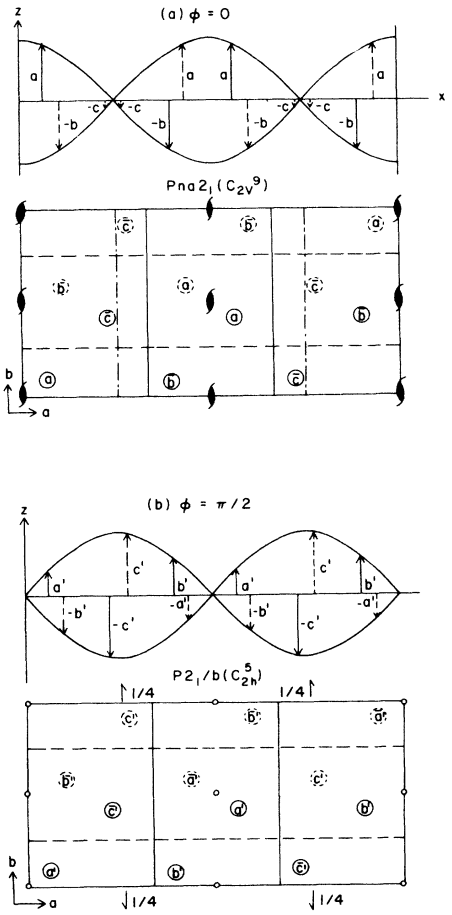

FIG. 16. Displacements of K_α ions in the unit call of the F phase for $\phi = 0$ and $\frac{1}{2}\pi$. Crystal takes either of the two possible phases. Displacements are given by the first term in the Eq. (17) with the $\vec{S}_1$-type symmetry mode. Actual displacements are more complex but the space group of the F phase can be concluded from these simplified displacements. In case $\phi = 0$ the symmetry becomes $Pna2_1(C_{2v}^9)$ and in case of $\phi = \frac{1}{2}\pi$ it becomes $P2_1/b(C_{2h}^5)$. Potassium selenate is the former case.

readily determined by locating the symmetry elements of the structure. For the case $\phi = 0$ there are four elements: $\{E|0\}$, $\{C_{2z}|\frac{1}{2}\vec{c}\}$, $\{\sigma_x|\frac{1}{2}\vec{a}_L + \frac{1}{2}\vec{b} + \frac{1}{2}\vec{c}\}$, and $\{\sigma_y|\frac{1}{2}\vec{a}_L + \frac{1}{2}\vec{b}\}$ and we get C_{2v}^9 as a space group. For the case $\phi = \frac{1}{2}\pi$, $\{E|0\}$, $\{C_{2y}|\frac{1}{2}\vec{a}_L + \frac{1}{2}\vec{b}\}$, $\{I|0\}$, and $\{\sigma_y|\frac{1}{2}\vec{a}_L + \frac{1}{2}\vec{b}\}$ are the symmetry elements and C_{2h}^5 is the space group. Here the fractional translations associated with the symmetry operations are given with respect to the unit cell of the F phase. For the general values of ϕ only $\{\sigma_y|\frac{1}{2}\vec{a}_L + \frac{1}{2}\vec{b}\}$ is present except $\{E|0\}$, so the space group is C_s^2. In Sec. VII we will show that the free energy is minimized with respect to the phase by taking either $\phi = 0$ or $\frac{1}{2}\pi$. Hence the crystal must assume either a C_{2v}^9 or C_{2h}^5 low-temperature structure. The former is the polar orthorhombic space group, while the latter is the monoclinic space group with b as the unique axis. We will see in Sec. VI that these two cases correspond to the induced ferroelectricity and ferroelasticity, respectively. Potassium selenate, of course, represents the former case.

VI. DETERMINATION OF THE EIGENVECTOR OF THE SOFT MODE

The inelastic neutron-scattering intensity in a one-phonon process is very useful in establishing the nature of the mode.[18,19] The knowledge of the mode is important in this case in order to clarify the origin of the lattice instability.

The relative integrated intensities of the soft phonon at $\vec{q} = 0.31\vec{a}^*$ and at $T = 145$ K and those of the central peaks at $\vec{q} = 0.31\vec{a}^*$ and $T = 129$ K were measured about several different reciprocal-lattice points. They are compared with the integrated intensities of satellite reflections at 110 K in Fig. 17. The scales of each set of data are chosen in such a way to aid comparison. The proportionality among three sets is remarkably good. This means that the low-frequency fluctuation which causes the central peaks, the static atomic displacements occurring in the transformation, and the dynamical displacements associated with the soft phonon have

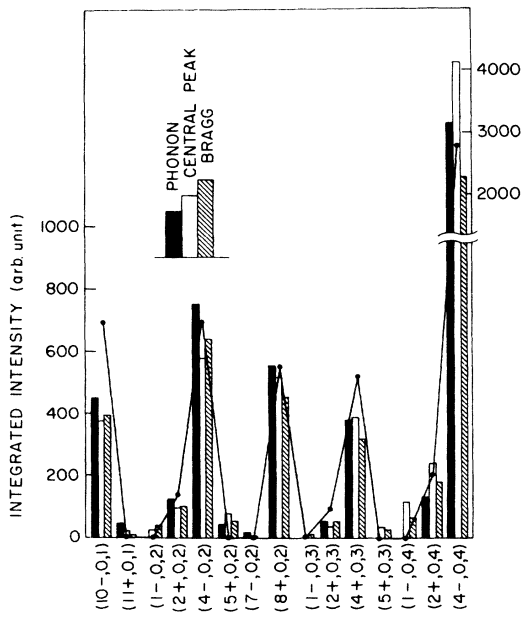

FIG. 17. Integrated intensities of the one-phonon scattering for the $q = 0.31$ soft phonon at 145 K, of the central components for the $q = 0.31$ spectra at 129 K, and of the superlattice reflections at 110 K. Scales of each set are adjusted in such a way as to aid comparison. Reflection indices refer to the low-temperature lattice. $(h\pm,k,l,)$ indicates $(h\pm\delta,k,l)$. Solid circles are the results for the best fitting Σ_2 mode.

a close similarity. We can therefore use any one of these three sets of intensity data to determine the eigenvector of the soft mode or the atomic displacements below T.

The inelastic structure factor in the expression of the one-phonon scattering at $\vec{K}=\vec{G}+\vec{q}$ by a molecular crystal is written

$$F_{in}(\vec{K})=\sum_{kp}\frac{\vec{K}\cdot\vec{\xi}_{kp}}{\sqrt{M_{kp}}}\,b_{kp}e^{-W_{kp}}e^{i(\vec{K}-\vec{q})\cdot\vec{x}(\ell)}e^{i\vec{K}\cdot\vec{X}(kp)} \tag{20}$$

under the rigid molecule assumption. In this formula b_{kp} and $e^{-W_{kp}}$ are the scattering length and the Debye-Waller factor of the atom p in the group k in the unit cell, respectively, and $\vec{\xi}_{kp}$ is the displacements amplitude of the atoms associated with the soft mode. As we saw in Sec. V, the displacement of the soft mode is written by the symmetry adopted eigenvectors which transform like Σ_2

$$\vec{\xi}_{kp}=\sum_{\lambda=1}^{6}S_\lambda(q)\,\vec{s}_{\lambda k}+\sum_{\lambda=7}^{10}S_\lambda(q)\,\vec{s}_{\lambda k}\times\vec{X}(kp)\,. \tag{21}$$

$S_\lambda(q)$'s are the amplitudes of the symmetry coordinates which are to be determined from the intensity measurements. Then structure factor (20) is rewritten as

$$F_{in}(\vec{K})=\sum_{\lambda}S_\lambda(\vec{q})\,f_\lambda(\vec{K})\,, \tag{22}$$

where

$$f_\lambda(\vec{K})=\begin{cases}\displaystyle\sum_{kp}b'_{kp}(\vec{K}\cdot\vec{s}_{\lambda k})e^{i\vec{G}\cdot\vec{x}(k)}e^{i\vec{K}\cdot\vec{X}(kp)} & \text{for } \lambda\le 6\,,\\ \displaystyle\sum_{kp}b'_{kp}\{\vec{K}\cdot[\vec{s}_{\lambda k}\times\vec{X}(kp)]\}e^{i\vec{G}\cdot\vec{x}(k)}e^{i\vec{K}\cdot\vec{X}(kp)} & \text{for } 7<\lambda\le 10\,,\end{cases} \tag{23}$$

are the structure factors for the symmetry modes, where $b'_{kp}=b_{kp}M_{kp}^{-1/2}e^{-W_{kp}}$. As we saw in Sec. V the symmetry modes for even λ are centrosymmetric and those for odd λ are anticentrosymmetric. Then we can write

$$f_\lambda(\vec{K})=\sum_{kp}b'_{kp}(\vec{K}\cdot\vec{E}_{\lambda kp})\times\{\sin[\vec{G}\cdot\vec{x}(k)]\cos[\vec{K}\cdot\vec{X}(kp)]+\cos[\vec{G}\cdot\vec{x}(k)]\sin[\vec{K}\cdot\vec{X}(kp)]\}\,, \tag{24}$$

for even λ and

$$f_\lambda(\vec{K})=\sum_{kp}b'_{kp}(\vec{K}\cdot\vec{E}_{\lambda kp})\times\{\cos[\vec{G}\cdot\vec{x}(k)]\cos[\vec{K}\cdot\vec{X}(kp)]-\sin[\vec{G}\cdot\vec{x}(k)]\sin[\vec{K}\cdot\vec{X}(kp)]\}\,, \tag{25}$$

for odd λ. In Eqs. (24) and (25) $\vec{E}_{\lambda kp}$ stands for $\vec{s}_{\lambda k}$ or $\vec{s}_{\lambda k}\times\vec{X}(kp)$ according to λ. Now the phonon or the central peak intensities are given by

$$|F_{in}(\vec{K})|^2=\Big(\sum_{\text{odd}}S_\lambda f_\lambda(\vec{K})\Big)^2+\Big(\sum_{\text{even}}|\mathrm{Im}S_\lambda|\,f_\lambda(\vec{K})\Big)^2\,. \tag{26}$$

We cannot solve this equation straightforwardly from the observed intensities because of the lack of the phase information. We can, however, apply a least square procedure to fit Eq. (26) to the intensity data. The results of the fitting are given in Table V and the fitted phonon intensities are shown in Fig. 17. In the course of the iteration we noticed that the magnitudes of S_7, S_8, and S_9 are very small and are negligible within the error of the fitting. They are therefore set to zero at the final stage of the fitting.

In order to sketch out the mode the values in Table V are conveniently replaced by their approximate values:

$$S_1=|\mathrm{Im}S_2|=1\,,\quad -S_3=-|\mathrm{Im}S_4|=S_5=0.5\,,\quad |\mathrm{Im}S_{10}|=0.1\,,\quad S_6=S_7=S_8=S_9=0\,. \tag{27}$$

This pattern of the atomic displacement with wave vector $\vec{q}_{1/3}$ is depicted in Fig. 18. In this figure, a unit cell is divided into three layers (I, II, and III) perpendicular to the $\vec{b}$ axis and the projections on the (a,c) plane of each layer are shown separately. The origin of the instability of this mode is not readily recognizable from this pattern. The mode is a complicated motion consisting of translations in the z direction of all the constituents and librational motions of the SeO_4 groups around the y axis. The coupling between the translations of K_α atoms and the rotations of SeO_4 groups as is clearly visible in the (II) layer may possibly give an intuitive clue to the instability of the nearest-neighbor interlayer forces.

TABLE V. Symmetry coordinate components determined from the one-phonon scattering intensities shown in Fig. 15.

Components	Fitted values
S_1	0.73 ± 0.03
$\lvert\mathrm{Im}S_2\rvert$	0.48 ± 0.04
S_3	-0.23 ± 0.02
$\lvert\mathrm{Im}S_4\rvert$	-0.34 ± 0.06
S_5	0.27 ± 0.01
$\lvert\mathrm{Im}S_6\rvert$	0.05 ± 0.006
S_7	0
$\lvert\mathrm{Im}S_8\rvert$	0
S_9	0
$\lvert\mathrm{Im}S_{10}\rvert$	0.07 ± 0.007

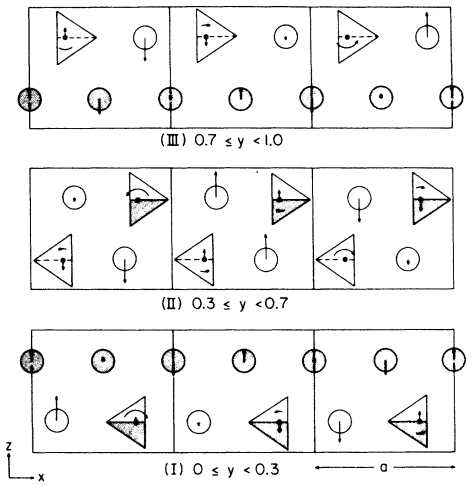

FIG. 18. Soft mode determined by analyzing one-phonon scattering intensities. Unit cells are divided into three layers (I, II, III) perpendicular to the $\vec{b}$ axis and the projection on the (a,c) plane are shown for each layer. Three unit cells along the axis are the full wavelength of the mode. Open circles indicate K_α ions, shaded circles K_β ions.

VII. LANDAU THEORY OF THE PHASE TRANSITIONS IN K_2SeO_4

A. Theoretical considerations

We wish to explain the successive phase transformations in K_2SeO_4, especially the incommensurate–commensurate phase transition, by a power-series expansion of a free-energy function with respect to the primary and secondary order parameters. The primary order parameter is the amplitude of lattice distortion $Q(\vec{q}_\delta, \Sigma_2)$ which is characterized by the wave vector $\vec{q}_\delta$ and by the irreducible representation Σ_2. We wish to use the spontaneous polarization along z, P_z, as the secondary order parameter. However, we will see that it must be generalized in such a way that the coupling term satisfies the translational symmetry of the lattice.

Higher-order terms in the expansion are in general of the form

$$V^{(n)}(\vec{q}_1 j_1, \vec{q}_2 j_2, \ldots, \vec{q}_n j_n)\, Q(\vec{q}_1 j_1) Q(\vec{q}_2 j_2) \cdots, Q(\vec{q}_n j_n), \tag{28}$$

where $V^{(n)}(\vec{q}_1 j_1, \vec{q}_2 j_2, \ldots, \vec{q}_n j_n)$ is an anharmonic coefficient[20] which may be nonvanishing only when

$$\vec{q}_1 + \vec{q}_2 + \cdots + \vec{q}_n = \vec{G}, \tag{29}$$

where $\vec{G}$ is a reciprocal-lattice vector or zero. This is required by the translational invariance. Moreover, the other symmetry elements of the space group restrict the type of products which arise in the power series. We are particularly interested in terms of the form $Q^{n-1}(\vec{q}_\delta, \Sigma_2)\, Q(\vec{q}', \Sigma')$. If such a term is present, the existence of a nonzero primary order parameter $Q(\vec{q}_\delta, \Sigma_2)$ guarantees the existence of a secondary *induced* order parameter $Q(\vec{q}, \Sigma')$ since it will always be possible to lower the free energy by a suitable choice of $Q(\vec{q}, \Sigma') \neq 0$. This is the mechanism of improper ferroelectricity and it has also been shown to be important in commensurate–incommensurate phase transformations in $NbSe_2$ and $TaSe_2$.[3] Such terms are responsible for both the lock-in transformation and ferroelectricity in K_2SeO_4.

The third-order term which involves square of $Q(\vec{q}_\delta, \Sigma_2)$:

$$V^{(3)}(\vec{q}_\delta\Sigma_2, \vec{q}_\delta\Sigma_2, \vec{q}'\Sigma')\, Q^2(\vec{q}_\delta\Sigma_2)\, Q(\vec{q}', \Sigma') \tag{30}$$

is nonvanishing only when

$$\vec{q}' = \vec{a}^* - 2\vec{q}_\delta = (1+2\delta)\tfrac{1}{3}\vec{a}^* \equiv \vec{q}_{2\delta} \tag{31}$$

and

$$\Sigma' = \Sigma_4 . \tag{32}$$

This term induces the secondary lattice distortion of Σ_4 type with the wave vector $\vec{q}_{2\delta}$ which causes "2δ" peaks in diffraction patterns as were observed. In $TaSe_2$ and $NbSe_2$ a similar third-order term proportional to $Q^2(\vec{q}_\delta, \Sigma_1)\, Q(\vec{q}_{2\delta}, \Sigma_1)$ produces coupling to a secondary order parameter on the same "soft branch" as the primary distortion. This term has a special symmetry in that the distinction between primary and secondary order parameters vanishes when $\delta = 0$. The expression given in Eq. (30) above, lacking this special symmetry, will tend to drive $\vec{q}_\delta$ either toward or away from commensurability [depending upon $\nabla_q \omega(q, \Sigma_4)$], and since it is not special at $\delta = 0$, it will not lead to lock-in. For these reasons we neglect this term and must search for another source of lock-in energy.

The fourth-order term which involves cube of $Q(\vec{q}_\delta, \Sigma_2)$

$$V^{(4)}(\vec{q}_\delta\Sigma_2, \vec{q}_\delta\Sigma_2, \vec{q}_\delta\Sigma_2, \vec{q}'\Sigma')\, Q^3(\vec{q}_\delta, \Sigma_2)\, Q(\vec{q}', \Sigma') \tag{33}$$

is interesting because it is special in the sense that

$$\vec{q}' = \vec{a}^* - 3\vec{q}_\delta = 3\delta\tfrac{1}{3}\vec{a}^* = \vec{q}_{3\delta}, \tag{34}$$

is very small and vanishes when $\vec{q}_\delta$ takes its commensurate value. Furthermore, an analysis of the space group symmetry shows that in this instance $\Sigma' = \Sigma_3$ to which both the transverse acoustic mode and the polar optic modes (both with polarization vectors along c) belong. First we consider only the polar optic modes as a secondary order parameter. Mention will be made of the acoustic mode later. For simplicity we consider only an appropriate linear combination of polar modes designated as $P_z(\vec{q}_{3\delta})$. This is a long-wavelength polarization

wave with vanishing net polarization as long as $\vec{q}_{3\delta}$ remains finite. When the primary lattice distortion becomes commensurate with the lattice periodicity, $P_z(\vec{q}_{3\delta})$ becomes $P_z(0)$, the macroscopic polarization. Thus we can explain how the spontaneous polarization is induced as a result of the incommensurate–commensurate phase transition.

Moreover, the term supplies a "umklapp energy" to drive the modulated structure towards the commensurate phase. In order to understand this point, we should pay attention to the requirement that all the terms which contain $\vec{q}$ belonging to the star of $\vec{q}$ are to be treated simultaneously in the expansion. In the present case the star of $\vec{q}_\Sigma$ is a pair of the wave vector $\vec{q}$ and $-\vec{q}$. As is proven in the appendix the fourth-order anharmonic coefficient $V^{(4)}(\vec{q}\,j, \vec{q}\,j, \vec{q}\,j, \vec{q}'j')$ has the following properties

$$\begin{aligned} V^{(4)}(-\vec{q}\,j, -\vec{q}\,j, -\vec{q}\,j, -\vec{q}'j') &= V^{(4)}(\vec{q}\,j, \vec{q}\,j, \vec{q}\,j, \vec{q}'j') \\ &= [V^{(4)}(\vec{q}\,j, \vec{q}\,j, \vec{q}\,j, \vec{q}'j')]^*, \end{aligned} \tag{35}$$

in case the crystal has an inversion symmetry. Hence the free-energy expansion is written

$$\begin{aligned} F = F_0 &+ A_1[Q(\vec{q}_\delta)\, Q^*(\vec{q}_\delta) + Q(-\vec{q}_\delta)\, Q^*(-\vec{q}_\delta)] \\ &+ A_P[P_z(\vec{q}_{3\delta})\, P_z^*(\vec{q}_{3\delta}) + P_z(-\vec{q}_{3\delta})\, P_z^*(-\vec{q}_{3\delta})] \\ &+ B_P[Q^3(\vec{q}_\delta)\, P_z(\vec{q}_{3\delta}) + Q^3(-\vec{q}_\delta)\, P_z(-\vec{q}_{3\delta})] \\ &+ C[Q(\vec{q}_\delta)\, Q^*(\vec{q}_\delta)]^2 + D[Q(\vec{q}_\delta)\, Q^*(\vec{q}_\delta)]^3 + \cdots, \end{aligned} \tag{36}$$

where F_0 is the free energy of the undistorted structure. Hereafter the indices for the irreducible representation are omitted on the understanding that the primary order parameter $Q(q_\delta)$ belongs to the Σ_2 representation and the secondary order parameter $P_z(q_\delta)$ belongs to the Σ_3 representation. It is important to note that at the commensurate phase $\vec{q}_{3\delta} = 0$ is special in that it does not have two arms in the star. Therefore the free energy of the commensurate phase becomes

$$\begin{aligned} F_{\text{comm}} = F_0 &+ A_1[Q(\vec{q}_{1/3})\, Q^*(\vec{q}_{1/3}) + Q(-\vec{q}_{1/3})\, Q^*(-\vec{q}_{1/3})] \\ &+ A_P P_z^2 + B_P[Q^3(q_{1/3}) + Q^3(-q_{1/3})]P_z \\ &+ C[Q(\vec{q}_{1/3})\, Q^*(\vec{q}_{1/3})]^2 + D[Q(q_{1/3})\, Q^*(q_{1/3})]^3. \end{aligned} \tag{37}$$

The energy required to generate the equilibrium polarization wave in the lattice drops to one half by going to the commensurate phase. This discontinuous decrease of the polarization energy locks in the commensurate phase.

We express the lattice distortions in terms of real amplitudes and phases by

$$\begin{aligned} Q(\vec{q}_\delta) &= \eta_1 e^{i\phi_1} \quad (\eta_1 > 0), \\ P_z(\vec{q}_{3\delta}) &= \eta_P e^{i\phi_P} \quad (\eta_P > 0). \end{aligned} \tag{38}$$

Then the free energy in the incommensurate phase is written

$$\begin{aligned} F_{\text{incomm}} = F_0 &+ 2A_1\eta_1^2 + 2A_P\eta_P^2 + 2B_P\cos(3\phi_1 + \phi_P)\eta_1^3\eta_P \\ &+ C\eta_1^4 + D\eta_1^6 + \cdots. \end{aligned} \tag{39}$$

This is minimized with respect to ϕ_1, ϕ_P, and η_P when

$$3\phi_1 + \phi_P = 0 \text{ or } \pi \tag{40}$$

and

$$\eta_P = (|B_P|/2A_P)\eta_1^3. \tag{41}$$

$3\phi_1 + \phi_P$ takes the value 0 or π according to whether B_P is negative or positive. Substituting Eqs. (40) and (41) into Eq. (39) we get

$$F_{\text{incomm}} = F_0 + 2A_1\eta_1^2 + C\eta_1^4 + (D - B_P^2/2A_P)\eta_1^6 + \cdots. \tag{42}$$

The term $(-B_P^2/2A_P)\eta_1^6$ constitutes the "umklapp energy" which comes from the balance of the polarization energy required to generate the secondary lattice distortion and the interaction energy between the primary and the secondary lattice distortions. If we neglect sixth order terms in this expression in minimizing with respect to η_1, which should be valid near T_i, we find

$$\eta_1 = 0 \text{ or } \eta_1 = \pm(-A_1/C)^{1/2}, \tag{43}$$

the former being an unstable solution for $T < T_i$. We assume that around $q_{\delta 0}$

$$\begin{aligned} A_1(T, \vec{q}_\delta) &= \alpha_1'(T - T_i) + \beta_1'(q_\delta - q_{\delta 0})^2 \\ &= \alpha_1 + \beta_1(\delta - \delta_0)^2, \end{aligned} \tag{44}$$

where α_1' and β_1' are positive constants and

$$\vec{q}_{\delta 0} = (1 - \delta_0)\tfrac{1}{3}\vec{a}^* \tag{45}$$

is the wave vector which characterizes the superlattice at T_i. Then

$$\eta_1 = \pm[(\alpha_1'/C)(T_i - T) - (\beta_1/C)(\delta - \delta_0)^2]^{1/2}. \tag{46}$$

We further assume that

$$A_P = \alpha_P + \beta_P' q_{3\delta}^2 = \alpha_P + \beta_P\delta^2 \tag{47}$$

and $\alpha_P \gg \beta_P\delta^2$. Then the free energy is minimized when $\partial F_{\text{incomm}}(\delta)/\partial\delta = 0$ or

$$\delta \approx \frac{\delta_0}{1 + (B_P^2\beta_P/4\alpha_P^2\beta_1)\eta_1^4}. \tag{48}$$

In order to get the temperature dependence of δ and η_1 exactly, Eqs. (46) and (48) should be solved simultaneously. But very close to T_i we may neglect the second term in Eq. (46) and we get

$$\eta_1 = (\alpha_1'/C)^{1/2}(T_i - T)^{1/2} \tag{49}$$

and

$$\delta = \delta_0/[1+\gamma(T_i - T)^2], \tag{50}$$

where

$$\gamma = B_p^2\alpha_1'^2\beta_p/4\alpha_p^2\beta_1 C^2. \tag{51}$$

The temperature dependence of δ depends upon the sign of β_p. If $\beta_p<0$, δ increases as the temperature decreases. In this case where the lattice can decrease the polarization energy by increasing δ, the crystal is not driven toward the commensurate–ferroelectric phase. On the contrary, if $\beta_p>0$, δ moves to zero asymptotically, that is, the superlattice tends to be commensurate.

The free energy for the commensurate superlattice given in Eq. (37) can be rewritten

$$F_{\text{comm}} = F_0 + 2A_{10}\eta_{10}^2 + A_{p0}P_z^2 + 2B_p\cos 3\phi_{10}\eta_{10}^3 P_z + C\eta_{10}^4 + D\eta_{10}^6 + \cdots . \tag{52}$$

This is minimized with respect to P_z and ϕ_{10} by

$$3\phi_{10} = 0 \text{ or } \pi,\ P_z = (|B_p|/A_{p0})\eta_{10}^3. \tag{53}$$

This choice of the phase was already used in Sec. V in order to derive the space group of the F phase. Inserting Eq. (53) back into Eq. (52) we get

$$F_{\text{comm}} = F_0 + 2A_{10}\eta_{10}^2 + C\eta_{10}^4 + (D - B_p^2/A_{p0})\eta_{10}^6 + \cdots . \tag{54}$$

If we neglect the sixth-order term and minimize F_{comm} with respect to η_{10},

$$\eta_{10} = \pm[(\alpha_1'/C)(T_i - T) - (\beta_1/C)\delta_0^2]^{1/2}. \tag{55}$$

This corresponds to Eq. (46). The next question is under what condition the incommensurate–commensurate transition occurs. We assume it occurs at the temperature for which the second terms in Eqs. (46) and (55) are negligible compared with the first term. After some algebra we can show that F_{comm} becomes less than F_{incomm} and the transition to the commensurate phase takes place at $T = T_c$ given as a solution of

$$\frac{B_p^2\alpha_1'^2}{4\alpha_p\beta_1 C^2}(T_i - T_c)^2 - \delta_0^2\frac{1+2\gamma(T_i - T_c)^2}{[1+\gamma(T_i - T_c)^2]^2} = 0. \tag{56}$$

The deviation δ jumps from

$$\delta_c = \delta_0/[1+\gamma(T_i - T_c)^2] \tag{57}$$

to zero and the spontaneous polarization appears with a finite value given by

$$P_z(T_c) = (\alpha_1'^{3/2}|B_p|/\alpha_p C^{3/2})(T_i - T_c)^{3/2}. \tag{58}$$

This transition is, therefore, of the first order. Below T_c the polarization is proportional to $(T_i - T)^{3/2}$.

As mentioned earlier, there is a further possible complication in the form of yet another permissible secondary order parameter. This is the strain component S_{xz} which is related to the Σ_3 acoustic phonon along $\vec{a}^*$ by

$$S_{xz} = \lim_{q\to 0}\Big(\sum_k e_z(k|\vec{q}\Sigma_3 a)\Big) iq_x Q(q\Sigma_3 a). \tag{59}$$

It is necessary to consider the strain wave with wave vector $\vec{q}_{3\delta}$ in the incommensurate phase as was the case for the polarization wave. Its amplitude is designated by $S_{xz}(\vec{q}_{3\delta})$. By a symmetry argument the coupling term linear in the strain wave and cubic in the order parameter $Q(\vec{q}_\delta, \Sigma_2)$ takes the following form

$$F_{\text{int}} = iB_s[Q^3(\vec{q}_\delta, \Sigma_2)S_{xz}(\vec{q}_{3\delta}) - Q^3(-\vec{q}_\delta, \Sigma_2)S_{xz}(-\vec{q}_{3\delta})], \tag{60}$$

where B_s is the real coefficient which is almost constant for small q. Adding this term to Eq. (36) and expressing order parameters by real amplitudes and phases, we can write the free energy in the incommensurate phase

$$F_{\text{incomm}} = F_0 + 2A_1\eta_1^2 + 2A_p\eta_p^2 + 2A_s\eta_s^2 + 2B_p\cos(3\phi_1 + \phi_p)\eta_1^3\eta_p + 2B_s\sin(3\phi_1 + \phi_s)\eta_1^3\eta_s + C\eta_1^4 + D\eta_1^6 + \cdots , \tag{61}$$

where the suffices p and s indicate the polarization wave and strain wave, respectively. By definition [Eq. (59)] A_s is proportional to the square of the sound velocity and is almost constant for small q. Minimization with respect to ϕ_p is realized when

$$3\phi_1 + \phi_p = 0 \text{ or } \pi \tag{62}$$

corresponding to $B_p<0$ or $B_p>0$ and minimization with respect to ϕ_s is realized when

$$3\phi_1 + \phi_s = \tfrac{1}{2}\pi \text{ or } \tfrac{3}{2}\pi \tag{63}$$

corresponding to $B_s<0$ or $B_s>0$. Although ϕ_1 is not determined in the incommensurate phase, there is a phase shift of $\frac{1}{2}\pi$ between the polarization wave and the strain wave. Setting $\partial F/\partial\eta_p = 0$ and $\partial F/\partial\eta_s = 0$ we get Eq. (41) and a similar result for η_s,

$$\eta_s = (|B_s|/2A_s)\eta_1^3. \tag{64}$$

In the incommensurate phase both kinds of secondary distortion coexist. Which is dominant is decided by the relative magnitudes of the "umklapp energy," $|B_s|^2/A_s$ to $|B_p|^2/A_p$. The existence of the strain wave does not alter the temperature dependence of δ given in Eq. (50), because the elastic energy required to generate the strain wave is independent of δ for small q and hence the system cannot gain energy by making δ small.

In the commensurate phase the free energy becomes

$$F_{\rm comm} = F_0 + 2A_{10}\eta_{10}^2 + A_{p0}\eta_{p0}^2 + A_{s0}\eta_{s0}^2 + 2B_p \cos 3\phi_{10}\eta_{10}^3 P_z + 2B_s \sin 3\phi_{10}\eta_{10}^3 S_{xz} + C\eta_{10}^4 + D\eta_{10}^6 + \cdots , \quad (65)$$

$\partial F_{\rm comm}/\partial\phi_{10} = 0$ gives

$$\tan 3\phi_{10} = B_s S_{xz}/B_p P_z . \quad (66)$$

We can, therefore, minimize $F_{\rm comm}$ by choosing

$$\cos 3\phi_{10} = -|B_p| P_z/(B_p^2 P_z^2 + B_s^2 S_{xz}^2)^{1/2} \quad (67)$$

and

$$\sin 3\phi_{10} = -|B_s| S_{xz}/(B_p^2 P_z^2 + B_s^2 S_{xz}^2)^{1/2} . \quad (68)$$

Substitution of Eqs. (67) and (68) into Eq. (65) gives

$$F_{\rm comm} = F_0 + 2A_{10}\eta_{10}^2 + A_{p0}P_z^2 + A_{s0}S_{xz}^2 + 2(B_p^2 P_z^2 + B_s^2 S_{xz}^2)^{1/2}\eta_{10}^3 + C\eta_{10}^4 + D\eta_{10}^6 + \cdots , \quad (69)$$

which is minimized with respect to P_z and S_{xz} by the conditions

$$P_z\left(A_{p0} - \frac{B_p^2\eta_1^3}{(B_p^2 P_z^2 + B_s^2 S_{xz}^2)^{1/2}}\right) = 0 \quad (70)$$

and

$$S_{xz}\left(A_{s0} - \frac{B_s^2\eta_1^3}{(B_p^2 P_z^2 + B_s^2 S_{xz}^2)^{1/2}}\right) = 0 \quad (71)$$

There are four solutions: (i)

$$P_z = S_{xz} = 0 , \quad (72)$$

which is an unstable solution for $T < T_i$. (ii)

$$P_z = 0 \quad \text{and} \quad S_{xz} = (|B_s|/A_{s0})\eta_{10}^3 , \quad (73)$$

which is realized when the "umklapp energy" for the strain is larger than that for the polarization,

$$B_s^2/A_{s0} > B_p^2/A_{p0} . \quad (74)$$

In this case the phase of the primary distortion is $\frac{1}{2}\pi$ or $\frac{3}{2}\pi$ and the spontaneous strain S_{xz} develops in the crystal whose symmetry becomes C_{2h}. This case coincides with the space group assigned for $\phi_{10} = \frac{1}{2}\pi$ in Sec. V.

(iii) In the opposite case where

$$B_s^2/A_{s0} < B_p^2/A_{p0} , \quad (75)$$

the phase $\phi_{10} = 0$ or π and the spontaneous polarization given by Eq. (26) develops and there is no spontaneous strain.

(iv) Both the spontaneous polarization and strain can coexist in the boundary case

$$B_s^2/A_{s0} = B_p^2/A_{p0} . \quad (76)$$

But this equality is realized only accidentally. In K_2SeO_4, case (iii) is realized.

B. Comparison with experiments

The theory developed above accomplishes our primary purpose to expose the physics underlying the successive phase transitions and occurence of the ferroelectricity. It is further interesting to test a quantitative applicability of the theory by the comparison with experimental results. In the comparison it should always be kept in mind that the theory is applicable only near the transition temperature T_i, because we neglected higher-order terms in the expansion.

The temperature dependence of the modulus of the primary order parameter η_1 is given by Eq. (49). This is to be compared with the intensity of the satellite reflection which is proportional to η_1^2. Experimental results shown in Fig. 5 follow

$$\eta_1^2 \sim (T_i - T)^{0.8\pm0.1}$$

down to 15 K below T_i.

The mean-field value of this exponent is of course $2\beta = 1.0$, but it may be of interest to point out in this connection that if we suppress the secondary order parameter, Eq. (36) is an example of a Landau–Ginzburg–Wilson Hamiltonian with an $(n = 2)$-component vector. We might therefore expect the true critical behavior of K_2SeO_4 to be that of the XY model, for which $2\beta = 0.67$. It would be of some interest to determine β (as well as the other critical indices associated with the 130 K phase transformation) more carefully in order to test this prediction.

The temperature dependence of δ given by Eq. (48) or by Eq. (50) has been compared with the experiments in Fig. 4, where the solid line was calculated by Eq. (48) with the coefficient of η_1^4 in the denominator being set equal to 0.025 and the satellite reflection intensity shown in Fig. 5 as a function of temperature was used to determine the temperature dependence of η_1^2. The dashed line was calculated by Eq. (50) with $\gamma = 0.002$ and $T_i = 127.5$ K. For both curves δ_0 is taken to be 0.07.

Figure 11 provides experimental support for the role of the "umklapp" term. Although there is an intrinsic temperature dependence of δ of dynamical origin, the values of δ realized in the incommensurate structure clearly depart from the intrinsic tendency indicating the effect of the "umklapp" energy.

We are unable to make a meaningful test of Eq. (53) relating P_z to η_{10} because the range of variation η_{10} is so small in the ferroelectric phase. In this connection, it is an extremely important and interesting test of our understanding of K_2SeO_4 to

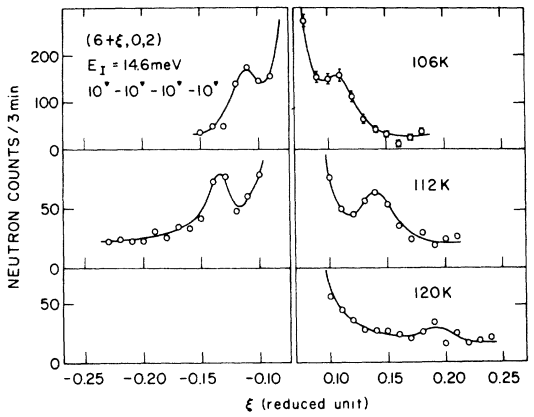

FIG. 19. "3δ" peaks observed around (602).

look directly for the sinusoidal polarization predicted for $T_c < T < T_i$. We expect to see satellite diffraction peaks close to the fundamental Bragg reflections. The wave vector characterizing these satellites is given by Eq. (3) and is very small; just above T_c the wavelength should reach a maximum $\sim 50a \sim 400$ A. It is technically difficult to observe a very weak peak on a tail of an adjacent intense peak. A tight collimation (10′– 10′– 10′– 10′) made it possible to observe the "3δ" satellites around only a few fundamental reflections. Figure 19 shows a result of elastic scans along [100] at three temperatures between T_i and T_c. The intensity of the peaks is about 10^{-5} of those of strong "δ" peaks. The position of the peaks coincides with $\tilde{q}_{3\delta}$ calculated by using the values of δ shown in Fig. 4. It is likely that these "3δ" satellites are due to secondary lattice modulation with the wave vector $\tilde{q}_{3\delta}$. We could not, however, exclude the possiblity of these peaks being diffraction harmonics of the primary modulation, because we failed to collect sufficient structure factor data to decide this point.

VIII. CONCLUDING REMARKS

Our neutron-scattering studies have disclosed the nature of the lattice instability in potassium selenate. The results have general relevance to improper ferroelectrics on one hand to the recently aroused attention to incommensurate structures on the other hand.

Improper ferroelectrics are characterized by an interaction term between a primary order parameter and polarization in a free-energy expansion. We have shown that the improper ferroelectricity in this substance is described by the interaction term given in Eq. (1). Aizu[21] proposed to classify the improper ferroelectrics according to the index of faintness n which is the lowest possible power of the primary order parameter which couples to the polarization. According to this classification potassium selenate is a new type of improper ferroelectric with $n = 3$. There is, however, a special situation in this system. The induction of spontaneous polarization is suppressed by the incommensurability of the distorted structure. The wave vector which characterizes the modulated structure changes with temperature, taking an incommensurate value continuously. The polarization is "hidden" (not a macroscopic observable) until the wave vector takes a commensurate value.

The incommensurate structural phase transformation is an interesting problem under current study.[22] The incommensurate systems originating from charge-density–wave instabilities have been extensively studied. But they are not necessarily ideal substances to study general characteristics of the incommensurate structure, because the phonon softening is not complete [metal dischalcogenides,[3] TTF-TCNQ (Ref. 23)], the dispersion relations are extremely sharp (potassium cyanoplatinide, KCP)[24] and the true long-range order is lacking (KCP)[25]. As we have seen, the soft phonon in potassium selenate is well defined, shows complete softening and the dispersion relation changes rather slowly in the q space. We could observe a close correspondence between the phonon instability in the P phase and the incommensurate structure in the I phase. The effect of the "lock-in" energy in driving the crystal towards the commensurate structure and in bringing about the first-order transformation to the commensurate phase is also confirmed in this substance. The origin of the incommensurate lattice instability in K_2SeO_4 is not understood at present. We have suggested the phenomenological origin from the force constant analysis of the soft-mode dispersion relation, which we hope to give a key to disclose the microscopic basis of the instability. The long-range nature of the effective forces deserves special attention. The eigenvector of the soft phonon determined in Sec. VI will help to project out the relevant combination of the interatomic force constants.

A few substances with isomorphous structures show lattice instabilities of various kinds. It may be interesting to inquire if there is anything in common among them. Ammonium sulfate, $(NH_4)_2SO_4$, transforms from the paraelectric phase with $Pnam$ to the ferroelectric phase with $Pna2_1$ without changing the size of the unit cell. The phase transition has been interpreted[26] to be caused by the instability of a B_{1u} mode at the zone center, which presumably corresponds to the zone center end of the upper branch partially observed and

shown in Fig. 6. Peculiar dielectric properties of this substance were attributed to a small polar components of the mode. Ammonium fluoberyllate, $(NH_4)_2BeF_4$, undergoes two successive phase transformations. The superlattice reflections at the low-temperature phases[27] suggest the softening of the zone boundary mode at $(\frac{1}{2},0,0)$, which one might be tempted to relate to the X_2 phonon at the zone boundary of the Σ_2 branch. As was mentioned in Sec. IV the existence of the a glide in the high-temperature phase makes it more natural to consider dispersion relations along $(q_1,0,0)$ in the doubly extended zone. The zone boundary X point in the original zone is no longer a high-symmetry point in this extended zone. (Note that the frequencies at the X point do not give rise to the Van Hove anomalies.) Then there is no reason for a lattice instability to occur preferentially at this point. A lattice instability with an incommensurate wave vector, say $q_1=0.5-\delta$, is thus more probable than one with a commensurate wave vector, $q_1=0.5$. The interlayer force constant analysis presented in Sec. IV B suggests that the fourth-neighbor force constant, F_4, becomes dominant in the instability at the X point. The F_4 term alone gives $\omega=0$ at $q_1=0.5$. But there can be contributions from F_1 and other long-range forces as well and even a small amount of these contributions displaced the unstable point from $q_1=0.5$. So the realization of the commensurate phase is rather accidental in this case. We may well suspect that the intermediate phase of $(NH_4)_2BeF_4$ is incommensurate. If this is really the case, we can apply essentially the same argument to the successive phase transitions and the induction of the spontaneous polarization in this substance. In this case the interaction term given by Eq. (30) takes the part of Eq. (33) in the theory of K_2SeO_4. The secondary order parameter is now the polarization component which transforms according to the Σ_4 representation [Eq. (32)]. This is the component along the b axis, being in accordance with observation.

After most of the present paper was written, the paper by Sawada, Makita, and Takagi[28] came to our notice. They have successfully explained the mechanical twinning properties in $(NH_4)_2SO_4$ by assuming a hypothetical hexagonal phase above the paraelectric orthorhombic phase and pointed out that the hexagonal phase is a real existence in K_2SeO_4 above 745 K.[29] The probable space group is $P6_3/mmc$ with the hexagonal axis corresponding to the orthorhombic a axis. The hexagonal-orthorhombic phase transformation is an order-disorder type transformation. In the hexagonal phase the orientation of the SeO_4 tetrahedra with repect to the hexagonal axis is in perfect disorder taking up and down orientation with equal probability. In the orthorhombic phase the SeO_4 groups take an ordered alignment as shown in Fig. 1. The symmetry change is described by the M_4 representation at $\vec{q}=\frac{1}{2}\vec{b}_2$, where $\vec{b}_2$ is a reciprocal unit-cell vector perpendicular to the hexagonal axis.

We have developed the Landau theory by taking the P-phase structure as a reference in writing down a free-energy expansion with respect to the displacements. Alternatively, one can take the hexagonal structure as a prototype structure. This may simplify some aspects of the theory and may give a unified viewpoint on the whole series of lattice instabilities. It is, however, more convenient and straightforward to use the orthorhombic reference if we confine our attention to the low-temperature phase transitions as we did in the present studies.

Similar order-disorder transformations are known[30] in K_2MoO_4, K_2WO_4, and Rb_2WO_4 which have the same hexagonal structure in the high-temperature phase. It is especially interesting to note that their low-temperature structures are again incommensurate; the ordering of MoO_4 or WO_4 tetrahedra takes place with incommensurate wave vector perpendicular to the hexagonal axis. In K_2SeO_4 the incommensurate phase is characterized by the wave vector along the hexagonal axis.

ACKNOWLEDGMENTS

One of the authors (MI) thanks Y. Ishibashi, A. Sawada, and Y. Takagi for discussions on various problems mentioned in Sec. VIII.

APPENDIX I: SYMMETRY PROPERTIES OF THE ANHARMONIC COUPLING COEFFICIENTS $V^{(n)}(\vec{q}_1,j_1,\vec{q}_2,j_2,\ldots,\vec{q}_n j_n)$

For reasons of notational convenience we will specialize our argument to $n=3$. The full third-order anharmonic potential is of the form

$$U^{(3)}=\sum_{\substack{\alpha\beta\gamma\\ ll'l''\\ kk'k''}}\phi_{\alpha\beta\gamma}(lk,l'k',l''k'')u_{\alpha lk}u_{\beta l'k'}u_{\gamma l''k''}. \quad \text{(A1)}$$

If there is a symmery operation $\{S\,|\,\vec{v}(S)\}$, where S is inversion, we define its action as mapping the atomic site (l,k) into a new site (L,K) and thus $T\{S\,|\,\vec{v}(S)\}u_{\alpha lk}=-u_{\alpha LK}$ so that the rotational invariance of Eq. (A1) requires that

$$\phi_{\alpha\beta\gamma}(LK,L'K',L''K'')=-\phi_{\alpha\beta\gamma}(lk,l'k',l''k''). \quad \text{(A2)}$$

We also need the transformation properties of the normal mode eigenvectors, $\vec{e}(S\vec{q})=e^{i\theta}T\{S\,|\,\vec{v}(S)\}\vec{e}(q)$, which with conventional choice of phase, θ, gives[31]

$$e_\alpha(k\,|\,\vec{q}) = \phi(k,K)e_\alpha(K\,|\,-\vec{q})\,, \tag{A3}$$

where

$$\phi(k,K) = \exp i\vec{q}\cdot[\vec{x}(K) - s\vec{x}(k)]$$
$$= \exp i\vec{q}\cdot[S\vec{x}(l) - \vec{x}(L) + \vec{v}(S)]\,, \tag{A4}$$

the latter following from the definition $\vec{x}(L)+\vec{x}(K) = S\vec{x}(l)+S\vec{x}(k)+\vec{v}(S)$. Equation (A1) can be rewritten

$$U^{(3)} = \sum_{\vec{q}\vec{q}'\vec{q}''} V(\vec{q}\vec{q}'\vec{q}'')Q_{\vec{q}}Q_{\vec{q}'}Q_{\vec{q}''}\,\Delta(\vec{q}+\vec{q}'+\vec{q}'')\,, \tag{A5}$$

where

$$V(\vec{q}\vec{q}'\vec{q}'') \equiv \sum_{\substack{ll'l''\\ kk'k''\\ \alpha\beta\gamma}} \phi_{\alpha\beta\gamma}(lk,l'k',l''k'')$$
$$\times e_\alpha(k\,|\,\vec{q})\,e_\beta(k'\,|\,\vec{q}')\,e_\gamma(k''\,|\,\vec{q}'')$$
$$\times \exp i[\vec{q}\cdot\vec{x}(l)+\vec{q}'\cdot\vec{x}(l')+\vec{q}''\cdot\vec{x}(l'')]\,.$$

Equation (A5) can be rewritten using Eqs. (A2)–(A4) as

$$V(\vec{q}\vec{q}'\vec{q}'') = -\sum \phi_{\alpha\beta\gamma}(LK,L'K',L''K'')e_\alpha(K\,|\,-\vec{q})\,e_\beta(K'\,|\,-\vec{q}')\,e_\gamma(K''\,|\,-\vec{q}'')$$
$$\times \exp i[\vec{q}\cdot\vec{X}(L)+\vec{q}'\cdot\vec{X}(L')+\vec{q}''\cdot\vec{X}(L'')]\,e^{i(\vec{q}+\vec{q}'+\vec{q}'')\cdot\vec{v}(S)}$$
$$= -e^{i(\vec{q}+\vec{q}'+\vec{q}'')\cdot\vec{v}(S)}V(-\vec{q}-\vec{q}'-\vec{q}'') \tag{A6}$$

and the corresponding general result for general n is

$$V^{(n)}(\vec{q}_1,\ldots,\vec{q}_n)$$
$$= (-1)^n e^{i(\vec{q}_1+\cdots\vec{q}_n)\cdot\vec{v}(S)}V^{(n)}(-\vec{q}_1,\ldots,-\vec{q}_n)\,. \tag{A7}$$

If there are no additional degeneracies, time reversal symmetry requires that $\vec{e}(k\,|\,\vec{q}) = \vec{e}^*(k_-\,|\,\vec{q})$,[32] so that in addition to Eq. (A7)

$$V^{(n)}(\vec{q}_1,\ldots,\vec{q}_n) = V^{(n)}(-\vec{q}_1,\ldots,-\vec{q}_n)^*\,. \tag{A8}$$

Equation (35) follows from Eqs. (A7) and (A8) since for D_{2h}^{16}, $\vec{v}(S)=0$.

Note added in proof. The discussion on the incommensurability of the intermediate phase of $(NH_4)_2BeF_4$ has been substantiated.[32]

*Guest scientist from Japan Atomic Energy Research Institute, Tokai, Japan, now returned.

†Work at Brookhaven performed under the auspices of the U.S. Energy Research and Development Administration.

[1]See, for example, V. Dovorak, Ferroelectrics 7, 1 (1974).
[2]E. Pytte, Solid State Commun. 8, 2101 (1970).
[3]D. E. Moncton, J. D. Axe, and F. J. Di Salvo, Phys. Rev. Lett. 34, 734 (1975).
[4]R. Comés, S. M. Shapiro, G. Shirane, A. F. Garito, and A. J. Heeger, Phys. Rev. Lett. 35, 1518 (1975).
[5]Y. Yamada, I. Shibuya, and S. Hoshino, J. Phys. Soc. Jpn. 18, 1594 (1963).
[6]Y. Shiozaki, Ferroelectrics 2, 245 (1971).
[7]K. Aiki, K. Hukuda, and O. Matumura, J. Phys. Soc. Jpn. 26, 1064 (1969).
[8]K. Aiki and K. Hukuda, J. Phys. Soc. Jpn. 26, 1066 (1969).
[9]A. Kalman, J. S. Stephens, and D. W. J. Cruickshank, Acta Crystallogr. B 26, 1451 (1970).
[10]N. Ohama, Mat. Res. Bull. 9, 283 (1974).
[11]K. Shimaoka, N. Tsuda, and Y. Yoshimura, Acta Crystallogr. A Suppl. 28, 187 (1972).
[12]K. Aiki, K. Hukuda, H. Koga, and T. Kobayashi, J. Phys. Soc. Jpn. 28, 389 (1970).
[13]H. Terauchi, H. Takenaka, and K. Shimaoka, J. Phys. Soc. Jpn. 39, 435 (1975).
[14]This value was read from Fig. 5 of Ref. 13. However, judging from the width of the triangle, showing the instrumental resolution, we guess that the scale of abscissa of this figure may be incorrect by a factor of 10. Then the disagreement in the distributions along $\vec{c}^*$ almost disappears.
[15]S. M. Shapiro, J. D. Axe, and G. Shirane, Phys. Rev. B 6, 4332 (1972).
[16]O. V. Kovalev, *Irreducible Representations of the Space Groups* (Gordon and Breach, New York, 1965).
[17]N. F. M. Henry and K. Lonsdale, *International Tables for X-Ray Crystallography*, Vol. I (Kynoch Press, Birmingham, 1952).
[18]J. Harada, J. D. Axe, and G. Shirane, Acta *Crystal*logr. A 26, 608 (1970).
[19]M. Iizumi, J. Phys. Soc. Jpn. 33, 647 (1972).
[20]M. Born and K. Huang, *Dynamical Theory of Crystal Lattices* (Oxford U.P., London, 1954).
[21]K. Aizu, J. Phys. Soc. Jpn. 33, 629 (1972).
[22]J. D. Axe, Proc. Conf. Neutron Scattering CONF-760601-P1 (Oak Ridge National Laboratory, Oak Ridge, Tenn., 1976), Vol. I, p. 353.
[23]G. Shirane, S. M. Shapiro, R. Comès, A. F. Garito, and A. J. Heeger (unpublished).
[24]B. Renker, H. Rietsch, L. Pintschovius, W. Gläser, P. Brüesch, D. Kuse, and M. J. Rice, Phys. Rev. Lett. 30, 1144 (1973).
[25]J. W. Lynn, M. Iizumi, G. Shirane, S. A. Werner, and R. B. Saillant, Phys. Rev. B 12, 1154 (1975).
[26]A. Sawada, Y. Takagi, and Y. Ishibashi, J. Phys. Soc.

Jpn. 34, 748 (1973).
[27]Y. Makita and Y. Yamauchi, J. Phys. Soc. Jpn. 37, 1470 (1974).
[28]A. Sawada, Y. Makita, and Y. Takagi, J. Phys. Soc. Jpn. 41, 174 (1976).
[29]G. Gattow, Acta Crystallogr. 15, 419 (1962).
[30]A. J. van den Berg, F. Tuinstra, and J. Warczewski, Acta Crystallogr. B 29, 586 (1973).
[31]We follow the general notation and phase conventions introduced by A. A. Maradudin and S. H. Vosko, Rev. Mod. Phys. 40, 1 (1968). We have suppressed the group-theoretical classification of eigenvectors since it plays no part in the argument.
[32]M. Iizumi and K. Gesi, Solid State Commun. (to be published).

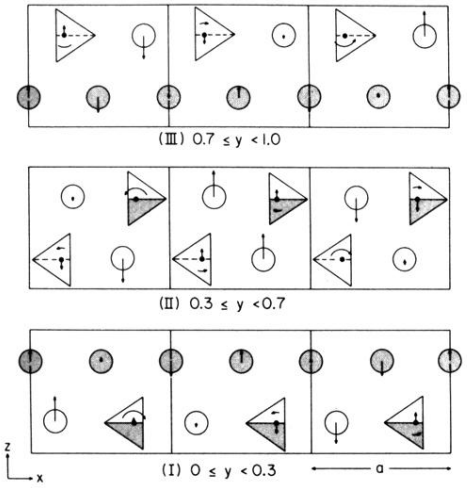

FIG. 18. Soft mode determined by analyzing one-phonon scattering intensities. Unit cells are divided into three layers (I, II, III) perpendicular to the $\vec{b}$ axis and the projection on the (a,c) plane are shown for each layer. Three unit cells along the axis are the full wavelength of the mode. Open circles indicate K_α ions, shaded circles K_β ions.